BJR

doi: 10.1259/bjr.20150185

Received: 3 March 2015 | Revised: 19 June 2015 | Accepted: 30 June 2015



Cite this article as:
Abou DS, Pickett JE, Thorek DLJ. Nuclear molecular imaging with nanoparticles: radiochemistry, applications and translation. *Br J Radiol* 2015; **88**: 20150185.

## NANOPARTICLES FOR DIAGNOSTIC IMAGING AND RADIOTHERAPY SPECIAL FEATURE: REVIEW ARTICLE

# Nuclear molecular imaging with nanoparticles: radiochemistry, applications and translation

**[1]D S ABOU, PhD, [1]J E PICKETT, PhD, [1,2]D L J THOREK, PhD**

[1]Division of Nuclear Medicine, Russell H. Morgan Department of Radiology and Radiological Sciences, The Johns Hopkins University School of Medicine, Baltimore, MD, USA
[2]Department of Oncology, The Sidney Kimmel Comprehensive Cancer Center, The Johns Hopkins University School of Medicine, Baltimore, MD, USA

Address correspondence to: Dr Daniel L J Thorek
E-mail: *dthorek1@jhmi.edu*

## ABSTRACT

Molecular imaging provides considerable insight into biological processes for greater understanding of health and disease. Numerous advances in medical physics, chemistry and biology have driven the growth of this field in the past two decades. With exquisite sensitivity, depth of detection and potential for theranostics, radioactive imaging approaches have played a major role in the emergence of molecular imaging. At the same time, developments in materials science, characterization and synthesis have led to explosive progress in the nanoparticle (NP) sciences. NPs are generally defined as particles with a diameter in the nanometre size range. Unique physical, chemical and biological properties arise at this scale, stimulating interest for applications as diverse as energy production and storage, chemical catalysis and electronics. In biomedicine, NPs have generated perhaps the greatest attention. These materials directly interface with life at the subcellular scale of nucleic acids, membranes and proteins. In this review, we will detail the advances made in combining radioactive imaging and NPs. First, we provide an overview of the NP platforms and their properties. This is followed by a look at methods for radiolabelling NPs with gamma-emitting radionuclides for use in single photon emission CT and planar scintigraphy. Next, utilization of positron-emitting radionuclides for positron emission tomography is considered. Finally, recent advances for multimodal nuclear imaging with NPs and efforts for clinical translation and ongoing trials are discussed.

## OVERVIEW OF NANOPARTICLES FOR IMAGING—ROLE OF PHYSICOCHEMICAL PROPERTIES AND BIOLOGICAL CHARACTERISTICS

For applications in biomedical imaging, desirable nanoparticle (NP) properties include robust imaging signal for a given modality, biocompatibility (and perhaps biodegradability) and versatility of surface chemistries, which can enable conjugation of ligands and/or bioactive structures. Generally, these requirements hold across modalities, including MR, optical, ultrasound and radioimaging. The chemical versatility of NPs enables multiple features to be available in a single agent. Functionality in the form of stealth-like coatings (to enable long circulation), affinity ligands (to enable targeted uptake), biodegradable constituents (to enable drug release and biocompatibility) and imaging or radiological detection (to enable long or short sensitive tracking and identification *in vivo*) is of great value. The biological fate of NPs can be modulated through primary design considerations and post-synthesis modification; particularly with respect to size, charge and hydrophylicity/phobicity characteristics. This is largely in contrast to small molecule radiotracers, which make up the bulk of probes used in nuclear medicine. NPs can effectively act as platforms allowing for a high degree of tailored modification for precise properties of interest. Additionally, NP radiosynthesis can be achieved with excellent radiolabelling efficiency and rapid synthesis and purification, which are often required for nuclear imaging applications utilizing short-lived radioisotopes.

For imaging applications, probe distribution is a key parameter. Pharmacokinetically, NP blood residency time and tissue uptake are predominantly dependent on size, surface chemistry and charge.[1] While targeting bioactive entities (such as conjugated peptides or conjugated antibodies) may enhance uptake to sites of disease, the hydrodynamic diameter critically determines residency time and clearance

routes. Parenterally administered, agents below the glomerular filtration cutoff (30–50 kDa or a diameter of approximately 5 nm) are rapidly excreted by the kidneys. Larger NPs may circulate longer, but often accumulate in the liver and spleen, while micron-sized particles become entrapped in capillary beds and the pulmonary vasculature. In response, the surfaces of the NPs are commonly modified with a polysaccharide or polymer, coatings which decrease recognition by passive and active clearance mechanisms, increase blood residency, circulation time and achieve greater uptake at sites of interest.

Furthermore, highly charged and hydrophobic particles are rapidly opsonized by serum proteins, a process that increases diameter and enhances recognition by the reticuloendothelial system (RES).[2] Below 100 nm in diameter, particles may circulate for longer, enabling sites of disease to be visualized through the enhanced permeability and retention effect (EPR).[3] This phenomenon results in non-specific accumulation of macromolecules and NPs at sites of compromised vasculature and blood flow—such as sites of malignancy. Beyond mere size, shape and aspect ratio (length:width) are also determinants of clearance route and kinetics.[1]

## Nanomaterials for biomedical imaging

A diversity of nanomaterials has been used for the purpose of nuclear imaging. These include lipids, proteins, carbon-based and metal-based particles. The following sections will briefly overview particle classes and their properties.

### *Liposomes*

Liposomes were first synthesized by Bangham[4] and are perhaps the longest studied NPs used for biomedical applications. These lipid structures are amphiphilic spherical vesicles, comprised of a phospholipid (PPL) bilayer or series of bilayers, and whose diameter may be tuned from 80 nm (unilamellar) to 1000 nm (multilamellar). Both hydrophilic and hydrophobic materials can be encased within liposomes. Polyethylene glycol (PEG) polymer coatings limit clearance and extend the circulation time in the blood by shielding the negative charges of the PPL heads.[5] Conversely, the same negative charges create a niche for electrostatic interactions, trapping positively charged isotopes or small molecules at the NP surface (Figure 1a–c).[6]

### *Quantum, silica and Cornell dots*

Quantum dots (QDs) are fluorescent nanocrystals (1–10 nm diameter) made of a combination of semi-conductor metals including: CdSe, Cds, CdTe, ZnSe, InP, InAs, PbSe (Figure 1d).[7,8] QDs have unique optical and electrical properties, such as bleach-free fluorescence and size-tuned emission characteristics. Composition, coating and size are determining factors of QDs emission wavelengths. CdSe, CdTe, InP, PbS and PbSe particles emit in the range of 470–660, 520–750, 620–720, 900 and 1000 nm, respectively. CdSe NPs emit at different wavelengths in a size-dependent manner: the smaller the particle, the shorter the emission wavelength.[9] Regarding blood circulation time, these small particles can be rapidly excreted.[10] Bare QDs are not always stable in aqueous or biological environments and can be coated by hydrophilic polymer layers such as PEG[11] or short-length peptides[12] for water-solubility, however, the increased NP size (>5 nm) sees a shift from renal to hepatic clearance.

Concerns about heavy metal toxicity of QDs hamper widespread use. More biocompatible particles have been developed using carbon[1] and also silica.[13] The latter has been used in Cornell dots (C-dots), which are ultrasmall particles (3–5 nm) consisting of a fluorophore encapsulated by a biodegradable shell of

Figure 1. Nanoparticle (NP) radiolabelling strategies: a variety of NP labelling approaches have been applied for imaging applications, as demonstrated using the lipid bilayer of liposomal NPs and quantum dot. (a) Radiometal chelation to the particle surface, using pre-formed particles. (b) Direct association of the radioisotope with the NPs surface (inset shows phosphate heads of surrounding lipids associating with a zirconium ion). (c) Entrapment of radioisotope or radiotracers within the core of a NPs. (d) Radioisotope may also be directly incorporated into particles during its formulation, such as $^{109}$Cd into a CdSe/ZnSe QD.[7] DPPC, 1,2-dipalmitoyl-sn-glycero-3-phosphocholine.

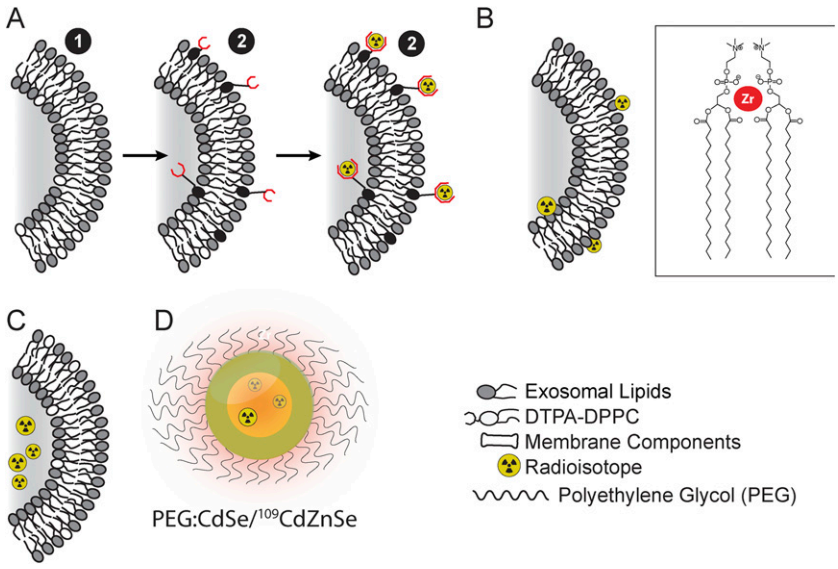

silica.[14] In contrast to QDs, which when PEG coated are re-routed to the liver,[11,15] C-dots are still rapidly excreted via glomerular filtration. Thus, the *in vivo* residency time is very short. This has potential advantages for radioactive dosimetry and long-term toxicity.[16,17]

### *Carbon-based nanoparticles*

Carbon nanotubes (CNTs) and graphene are both carbon-based materials with well-defined physical and chemical properties. CNTs can be singlewalled or multiwalled and of varying lengths.[18] These pure carbon materials can be chemically modified to enhance hydrophilicity and to enable functionalization via ligands or radiolabels.[19] To modify their surfaces, CNTs have been wrapped in polymeric chains, which can be held in place by high hydrophobic/philic adherence, electrostatic interactions or covalent linkages. Paradoxically, despite their long length (200–300 nm long), it has been shown that covalently functionalized CNTs can be cleared rapidly by renal filtration owing to their small diameter (only 1 nm).[19,20]

### *Polymeric nanoparticles*

Polymeric NPs are structures composed of block-copolymer chains (with linked "blocks" of different monomers). Rationally designed to self-assemble into spherical- or rod-shaped micelles,[21] these can be radiolabelled by encapsulating a radioactive agent in their core[22] or by labelling the polymer layer itself.[23] Polymersomes are self-assembled vesicles made of block-copolymers forming amphiphilic membranes—replicating the features of a lipid bilayer. The diameter of such particles can be controlled through mechanical extrusion, resulting in sizes as small as 200 nm with a narrow polydispersity index.[22]

Dendrimers are a well-studied family of controlled branched polymer macromolecules. The particles consist of sequential identical groups, a dendron, linked together. The number of these branched groups can be controlled, and therefore particle size can be carefully tailored, offering various degrees of hydrophilicity and/or functionalization.[24] For example, a fourth generation dendrimer, dubbed G4, would constitute four layers of interconnected dendrons, all constructed around a monomeric focal point.[25] For medical applications, the most common monomer investigated has been the hydrophilic ethylene diamine. This is polymerized into a polyamidoamine (PAMAM) dendrimer, offering terminal amino groups for conjugation of chelates or antibodies.[26] Furthermore, these groups are chemically labile, readily generating hydroxyls, carboxylic acids etc.

### *Inorganic nanoparticles*

Various approaches have been investigated to formulate stable inorganic NPs. The most common preparations for bioimaging applications are based on the suspension of heavy metals into nanocolloids, which are then stabilized by polymeric, polysaccharide or protein shells. These shells serve multiple functions: to stabilize the NPs, to enable further chemical modification, to reduce adverse biological events and/or to present radiolabelling sites. Among the most thoroughly investigated inorganic NPs are gold NPs (AuNPs; as well as other noble metals such as silver and platinum) and iron oxide NPs (IONPs).

AuNPs can be synthesized with tightly controlled size and aspect ratio (such as spheres or rods) using chemical reduction methods.[27] AuNPs have intrinsic optical properties enabling their use as nanodiagnostic materials for fluorescence detection or Raman spectroscopy of tumour cells.[28] A convenient chemical approach for surface modification utilizes the covalent bonding of Au to thiols, leading to conjugation of polymers ($PEG_{2000}$-SH),[29] fluorescent probes[30] or disease-targeting molecules, such as peptides,[31] antibodies[32] or nucleic acids.[33]

IONPs consist of an iron oxide core, with a tunable size ranging from several nanometres to microns, which can be synthesized using a range of techniques. The bare iron oxide core is commonly enveloped in macromolecular structures, including human serum albumin,[34] polylactic acid,[34] or, most frequently, cross-linked sugars such as dextran[35] or chitosan.[36] Functionalized polymeric coatings, including those used for cross-linked iron oxide,[37] offer surface chemistries for conjugation of targeting moieties[38] or chelates for radiolabels or optical/fluorescent probes.[39]

More recently, polymer-coated metallic core NPs formulated with silver or platinum–cobalt core support were radiolabelled with $^{125}$I (for AgNPs) or $^{11}$C (for Pt-based NPs).[40–43] Similarly, rare earth cationic assembly elements or upconversion nanophosphores consisting of $NaYF_4$, Yb, Er core associated with $Gd^{3+}$ and radioactive fluorine-18 ($^{18}$F) were reported for MR-PET multimodality imaging.[44]

## SINGLE PHOTON EMISSION CT AND PLANAR SCINTIGRAPHIC IMAGING WITH NANOPARTICLES

### Single photon emission computed tomography isotopes, physical properties and radiolabelling methods

Single-photon emission CT (SPECT) is the most clinically utilized nuclear medicine imaging technique.[45] Generally, it is used for qualitative assessment of cardiac function or detection of disease. However, recent advances have enabled quantitative, whole-body imaging of radionuclide distribution.[46] The most common isotopes utilized for SPECT imaging are the metastable technetium isotope $^{99m}$Tc, which has a relatively short half-life (6.1 h), and the longer-lived indium isotope $^{111}$In (2.8 days) (Table 1). Both radioisotopes present excellent γ emission properties for sensitive, high-resolution imaging, and $^{99m}$Tc is available from a convenient generator system.

### Chemistries for single photon emission CT nanoparticle labelling

A wide choice of radiolabelling strategies of NPs is available depending on the quality, compatibility and radiometal of NPs (Figure 1). The most straightforward approach consists in the direct radiolabelling of NPs through the addition of radioisotope during synthesis or utilizing chelator-free methods. Cases of iron oxide radiolabelling with $^{99m}$Tc-pertechnetate or $^{111}InCl^3$ trapped in the shell or nanocore demonstrate stable radioNPs.[47–49] Similarly, comixing $^{99m}$Tc-pertechnetate with sodium thiosulfate or human serum albumin proteins forms colloidal suspensions, namely $^{99m}$Tc-sulphur colloid[50] and $^{99m}$Tc-nanocoll.[51] The colloid size may be tuned through filtration.[52] Direct radiolabelling may be achieved for liposomes utilizing PPL electrostatic

Table 1. Single photon emission CT radioisotopes clinically and pre-clinically utilized for nanoparticle (NP) labelling

| Isotope | Half-life and most abundant γ energies (MeV) (% abundance) | Radiolabelling methods | Radiolabelled NPs |
|---|---|---|---|
| $^{99m}$Tc | 6.1 h<br>0.141 (89%) | HMPAO/glutathione | Liposomes |
| | | Bisphosphonates | IONPs |
| | | HYNIC | Liposomes |
| | | DTPA | Dendrimers |
| | | Direct radiolabelling | IONPs; sulfur-colloid |
| $^{111}$In | 2.8 days<br>0.245 (94%); 0.171 (90%); 0.023 (69%) | Oxine/nitrilotriacetic acid | Liposomes |
| | | CHX-DTPA | Liposomes |
| | | DOTA | Dendrimers |
| | | DTPA | AuNPs; liposomes |
| | | Direct radiolabelling | IONPs |
| $^{67}$Ga | 3.26 days<br>0.009 (36%); 0.185 (20%); 0.300 (16%) | NOTA | Cobalt-ferrite NP |
| | | DFO | Liposomes |
| | | DTPA | Liposomes |
| $^{125}$I | 60.1 days<br>0.036 (7%) | Tyrosine electrophilic substitution; iodogen or chloroamine-T catalysed | Liposomes |
| | | Bolton–Hunter reagent | Quantum dots |
| | | Direct NP radiolabelling | AgNPs; AuNPs |

AgNPs, silver NPs; AuNPs, gold NPs; CHX-DTPA, N-(2-amino-3-(4-isothiocyanatophenyl) propyl) cyclohexane-1,2-diamineN,N′,N′,N″,N″-pentaacetic acid; DFO, desferioxamine; DOTA, 1,4,7,10-tetraazacyclododecane-1,4,7,10-tetraacetic acid; HMPAO, hexamethyl propyleneamine oxime; HYNIC, hydrazinonicotinamide; IONPs, iron oxide NPs; NOTA, 1,4,7-Triazacyclononane-N,N′,N″-triacetic acid.

interactions or hydrophilicity/phobicity adherence to membranes (Figure 1).[53] However, limited *in vivo* stability has often been observed. Alternatively, liposomes may be radiolabelled either by extrusion in a radioisotope-containing fluid to entrap the isotope or via radioactive passive diffusion through membranes. The latter consists in the transportation of radioactive hydrophobic chelates through liposome membranes and entrapment of the radioisotope by transchelation in the aqueous cavity. As a result, the radioisotope is efficiently trapped in the intact vesicle (Figure 1).[54]

The most common NP radiolabelling approach with radiometals utilizes a two-step procedure in which chelates are first conjugated to pre-formed NPs, which are then subsequently labelled by mixing with the radioisotope (Figure 2). Although this approach may be chemically challenging to achieve high specific activity, chelation is often a preferred radiolabelling strategy owing to stable radiometal co-ordination with covalent linkage of the radiocomplex and the availability of numerous metal radionuclides (often without requirement of an on-site cyclotron). As an example, liposome surface chelation can be conducted modifying lipids by attachment of chelators on lipid hydrophilic heads[55–57] or at the end of PEG chains.[58,59]

Alternatively, NPs can be labelled via covalent radioiodination. Commercially available reagents chloramine-T and Iodogen can be used to oxidize radioiodide into a mixed halogen species, which readily iodinates activated aromatic groups via electrophilic substitution. This reaction is rapid enough for use with even the shortest-lived iodine isotopes. Many amino acid side groups can be labelled, most notably tyrosine.[60] However, if insufficient numbers are present, amines can be covalently linked to phenol via the Bolton–Hunter reagent[61] (Figure 3). Advantages of this chemistry include mild reaction conditions, regioselectivity and efficiency at room temperature, while generating very high specific activity. One limitation is that activated rings (such as phenol) are deiodinated *in vivo*, resulting in accumulation of radioiodine in the thyroid. However, consumption of iodine [from potassium iodide (KI) or kelp] beforehand will saturate the thyroid with non-radioactive iodine, thus reducing accumulation and exposure.

## Pre-clinical development

A significant volume of pre-clinical research has been conducted aiming to develop biocompatible, non-toxic NPs for detection and monitoring of disease. The versatility of chemical and detection approaches afforded utilizing γ-emitting radionuclides has made them a major focus for work with NPs. In this section of the review, we highlight the aspects of single photon-emitting radionuclides for planar and SPECT imaging.

### *Organic nanoparticles for single photon emission CT and planar imaging*

Among the earliest reports of radiolabelled NPs are attempts to use liposomal particles encapsulating $^{111}$In-complexes to identify tumours.[62] This early work demonstrated the potential

Figure 2. Radiometal complexes for single photon emission CT and positron emission tomography imaging of nanoparticles (NPs). Chemical structures of ligands used for radiolabelling using metal isotopes. These ligands have been used to chelate radioisotopes to be covalently conjugated to the NP surface, or to encapsulate activity within particles. BAT, 6-[p-(bromoacetamido)benzyl]-1,4,8,11-tetraazacyclotetradecane-N,N′,N″,N‴-tetraacetic acid; CHX-DTPA, N-(2-amino-3-(4-isothiocyanatophenyl)propyl)cyclohexane-1,2-diamine-N,N′,N′,N″,N″-pentaacetic acid; DCPA, dipicolylamine alendronate; DFO, desferrioxamine; $DO_3A$, 1,4,7-tris(carboxymethyl)-1,4,7,10-tetraazacyclododecane; DOTA, 1,4,7,10-tetraazacyclododecane-1,4,7,10-tetraacetic acid; $DTCBP_2$, pentasodium mono(3-hydroxy-3,3-diphosphonato-propyl(methyl)dithiocarbamate; HMPAO, hexamethylpropyleneamine oxime; HYNIC, 6-hydrozino-nicotinamide; NOTA, 1,4,7-triazacyclononane-N,N′,N″-triacetic acid; TETA, 1,4,8,11-tetraazacyclotetradecane-1,4,8, 11-tetraacetic acid.

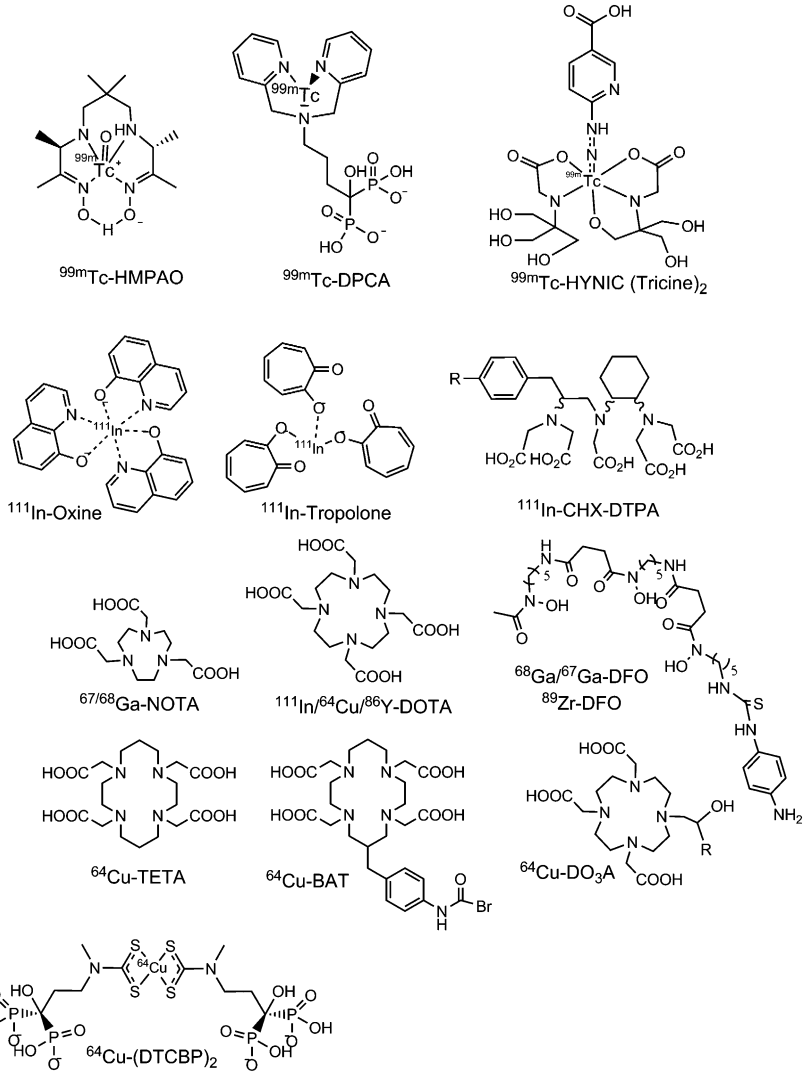


of this emerging technology, achieving tumour uptake values as high as 18.5% injected activity per gram (%IA/g) of tissue, using neutral-lipid structures. As well, $^{111}$In-labelled liposomes[63,64] and $^{99m}$Tc-liposomes[5,65–67] have been studied to identify active uptake at sites of infection and inflammation. A focus has been to extend the circulation time and enhance tumour targeting. Liposomes have been grafted with long PEG chains of varying length which demonstrate increased blood residency time up to 24 h p.i *vs* only 4 h for non-coated liposomes.[64] Molecularly specific targeting using antibody or peptide attachments to the NP surface has been investigated. Conjugation strategies have focused upon binding these molecules at the end of the PEG chains for reduced steric hindrance at the particle surface. Both immunoliposomes[68] and peptide-conjugated liposomes[69] demonstrated selective cell internalization *in vitro* and enabled tumour detection *in vivo*. However, greater and irreversible liver and spleen uptake was seen especially for immunoliposomes (30–40% IA/g), with limited gains above passive percent initial activity per gram at tumour tissues.

Polymersomes consist of block copolymers, which are long linear amphiphilic polymeric chains made of a hydrophilic and a hydrophobic portion. They can be tailored for specific applications and have greater stability in comparison to liposomes. Similarly to liposomes, polymersomes were radiolabelled with $^{111}$In, utilizing an

Figure 3. Fluorine-18 ($^{18}$F) and halogenation prosthetic groups: (a) $^{18}$F is the most widely utilized positron emission tomography radioisotope and has been applied to several nanoparticle (NP) formulations. Si-FASH, 4-(di-tert-butyl[$^{18}$F]fluorosilyl)benzenethiol. (b) Radioiodination and bromination can be readily accomplished for gamma emitting ($^{123}$I, $^{125}$I) and positron emitting ($^{124}$I, $^{76}$Br) radiosotopes.

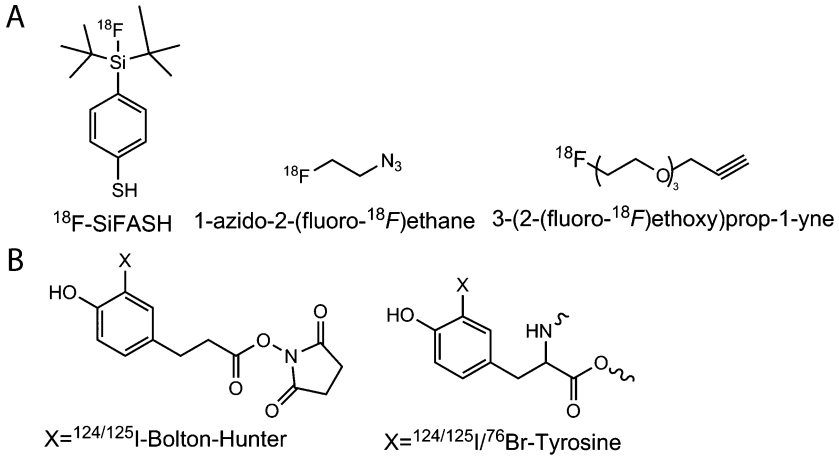


encapsulation approach. $^{111}$In-tropolone was incubated with preformed NPs that engulfed DTPA. $^{111}$In was transchelated and readily trapped by DTPA in the aqueous compartment.[22] This approach resulted in highly stable radiolabelled NPs with no detectable radioactive leakage as the polymer membrane is impermeable to its cargo.

Imaging of dendrimer NPs has focused on the well-characterized PAMAM family. The G4 particle, which presents 64 reactive amines, has been modified with the hydrazinonicotinamide (HYNIC) chelator for subsequent radiolabelling with $^{99m}$Tc. These NPs demonstrated significant liver, spleen and kidney uptake.[70,71] Similar distribution values have been reported for antibody-conjugated G4 dendrimer targeted to tumour antigens, with increased tumour uptake.[72] In comparison, smaller G2 particles possess a faster excretion rate.[2] The G2 particles have been functionalized with antibodies and the common radiometal chelator 1,4,7,10-tetraazacyclododecane-1,4,7,10-tetraacetic acid (DOTA), for labelling with $^{111}$In, $^{90}$Y or $^{88}$Y.[26,73] Finally, an alternative dendrimer scaffold of poly-diamidopropanoyl (PDAP) functionalized for both radiolabelling and tumour targeting has been used for imaging. PDAP dendrimer was dually targeted to pancreatic cancer cells by peptide and nucleic acid aptamer conjugation, as well as functionalized with the DOTA chelate. $^{111}$In-radiolabelling enabled evaluation by biodistribution and planar scintigraphy to show greater uptake for xenografts bearing the targeted epitope.[74]

CNTs have been widely investigated as fluorescent imaging and drug delivery platforms. The highly stable carbon–carbon bonds of the CNT can be directly functionalization using harsh chemical syntheses. Utilizing these methods, Das et al reported a dual-modality fluorescent/SPECT ($^{99m}$Tc) tumour-targeted multiwalled CNT (MWCNT) for therapy. Folic acid, methotrexate drug and the fluorophore AF-488/647 were conjugated to MWCNT. The construct was then radiolabelled with $^{99m}$Tc and a $SnCl_2$ reducing agent utilizing direct electrostatic interaction with the MWCNT surface. This direct approach resulted in nearly complete $^{99m}$Tc-radiolabelling efficiency and was seen to retain 85% of the label over 24 h p.i.[75]

### *Inorganic nanoparticles for single photon emission CT*

AuNPs have been directed to sites of disease by functionalization with small peptides such as modified bombesin for prostate cancer[76] or cyclic-RGDfK for imaging of tumour angiogenesis[77] and imaged with SPECT. These AuNPs were radiolabelled with $^{99m}$Tc using HYNIC chelation directly onto AuNPs via thiol binding. The particles sizes varied within 10–20 nm, with visible light absorbing wavelength (550 nm). Upon chemical modification of AuNPs one can use Raman spectrometry to confirm conjugation; providing a facile and robust method to characterize particles. RGD conjugated AuNPs resulted in a modest increase of tumour uptake (3% IA/g) as compared with non-targeted AuNPs (1.5% IA/g). $^{111}$In-DTPA-AuNP have been used as an imaging and distribution platform to study the effect of size, surface chemistry and PEG chain length on the stability and pharmacokinetics (PKs) of AuNPs. Long PEG chain (5K: 5000 molecular weight) conjugated to thioacetic acid on AuNPs exhibited higher stability as compared with shorter PEG chain length and direct thiol conjugation.[78] Furthermore, smaller NP size (20 nm) reduced retention by the RES, prolonging blood residency and circulation time.

More recently Bogdanov et al addressed issues of biocompatibility with AuNPs through surface chemistry modification. The PKs of AuNPs grafted with highly hydrophilic coatings composed of methoxypropylethylene glycol connected to polylysine were investigated. This particular coating was reported to decrease the immunogenicity and as such $^{99m}$Tc-methoxyPEG-polylysine-AuNP exhibited long blood residency time ($t_{1/2}$ = 17.2 h) and limited RES and kidney uptake.[79] While these efforts have sought to utilize the highly configurable AuNP platform for specific disease imaging with limited background distribution, a remaining limitation is the undefined *in vivo* long-term toxicity.[80,81] Finally, the use of radiolabelled IONPs for imaging will be addressed as a multimodality imaging agent later reported in this review (the Positron emission tomography/MR and single photon emission CT/MR nanoparticles Section).

### Clinically applied single photon emission CT nanoparticles for nuclear imaging

Despite broad pre-clinical efforts to develop clinically applicable NPs for SPECT, few formulations have made it to the stage of clinical evaluation nor approval by the Food and Drug Administration (FDA). One successful development is $^{99m}$Tc-colloid currently utilized for intraoperative guidance of lymph nodes resection in patients with melanoma and breast cancer. The first generation of $^{99m}$Tc-colloid was human serum albumin nanocolloid (or $^{99m}$Tc-Nanocoll).[82] Albeit approved in Europe for nodal detection, this radiopharmaceutical is not approved for use in the United States.[83] Instead, a modified formulation of colloid named $^{99m}$Tc-sulfur nanocolloid has been validated for the same medical purpose in patients presenting melanoma, prostate[51,84] and breast cancer.[85] Clinical trials of $^{99m}$Tc-sulfur nanocolloid are currently ongoing for lymph node visualization for resection in patients with rectal cancer (ClinicalTrials.gov identifier: NCT02112240) and patients with breast cancer (ClinicalTrials.gov identifier: NCT02287675).

An $^{111}$In-encapsulating liposome formulation, named Vescan, was clinically evaluated using SPECT imaging. Phase 3 clinical trials were conducted with the agent for detection of carcinoma and metastases of prostate, lung and breast cancer.[86–89] The same probe was also tested for identification of lesions of Kaposi sarcoma and lymphoma in patients with AIDS.[90] On average, the malignancy detection rate was around 70%, which was insufficient for FDA approval at the time (>85%).

Further translational liposome efforts have focused on the use of $^{99m}$Tc/$^{111}$In radiolabelled PEG-coated liposomes or so-called stealth liposomes. These were developed to result in prolonged blood circulation time to achieve higher tumour to background ratios by enhancing the EPR effect.[5,59,91] Stealth liposomes were clinically tested for the detection of infections and inflammations at low and high lipid dose. It was observed that low dose injection resulted in major radioactive accumulation in liver, spleen and bone marrow, in contrast to high dose remaining in blood circulation up to 24 h p.i. Intestinal radioactive accumulation proved hepatobiliary excretions of the digested particles.[5,91]

## POSITRON EMISSION TOMOGRAPHY WITH NANOPARTICLES

Positron emission tomography (PET) is a sensitive and quantitative tracking tool well suited for *in vivo* NP characterization. It provides relatively high resolution images (3–7 mm depending on scanners) of the radioactive distribution through organs with reduced scatter relative to planar and SPECT imaging. The determination of PK, clearance and toxicity of novel nanostructure designs are prerequisites for full pre-clinical and clinical development of any drug or imaging agent. The inherently quantitative PET modality is therefore ideally suited to study these features.

### Positron emission tomography isotopes, physical properties, radiolabelling methods

PET radiolabelling approaches consist of two main strategies: utilizing direct covalent chemistries or co-ordination chemistry.[92] Radioisotopes amenable to organic chemistry, including $^{11}$C and halogens like $^{18}$F, $^{76}$Br and $^{124}$I, are usually bound covalently, while radiometals are typically bound via chelation. Recent advances have been made which incorporate radiometals directly into or onto the NP for ligand-free radiolabelling approaches, detailed below. Produced by cyclotron bombardment of solid or gas targets ($^{13}$N, $^{11}$C, $^{18}$F-FDG, $^{64}$Cu, $^{76}$Br, $^{86}$Y, $^{89}$Zr and $^{124}$I) or by generator systems ($^{68}$Ga), these positron-emitting isotopes provide a wide range of chemistries and physical properties for imaging when coupled to NPs (Table 2).

### Chemistry for positron emission tomography radioisotopes nanoparticle labelling

NP radiolabelling with positron emitters is equally diverse to that of single photon emitting radionuclides. Considerations such as the nanostructure composition, stability and chemical functionality are important when selecting a PET isotope. Commonly, the choice of label is set according to the biological mechanism interrogated and the *in vivo* residency time of NPs.[97]

From a radiolabelling perspective, use of $^{11}$C and $^{18}$F-FDG or the halogens $^{124}$I and $^{76}$Br labelling is most often conducted by covalent binding directly onto the NP surface or to a spacer subsequently associated to NPs[97] (Figure 3). Short-lived $^{11}$C and $^{18}$F-FDG require fast and efficient radioparticle syntheses, and necessitate on-site cyclotron facilities, commonly limited to academic settings. These radioisotopes are convenient to define PKs and investigate biological events of short duration. For example, the short-lived $^{11}$C radiolabelling has been conducted by N-methylation of $^{11}$C-methyl iodine to amines grafted on iron oxide surface.[41]

$^{18}$F-FDG is the most commonly used PET isotope in the clinic as either $^{18}$F-FDG-NaF for bone scanning or as $^{18}$F-FDG. Its common use has led to the development of an array of chemistries for labelling, many of which have been adapted and applied to NPs. Fluorination may be conducted by:[92] nucleophile substitution of leaving groups such as aliphatic tosyle[98] or as ter-butyl-silicon construct.[99] With minimal chemical modification, it is also possible to introduce $^{18}$F-FDG by direct binding to the NP, exploiting fluorine's reactivity towards aluminium oxide or hydroxyapatite.[100] A major recent development in the field of radiofluorination has been the discovery of stable and efficient co-ordination with aluminium–1,4,7-Triazacyclononane-N,N′, N″-triacetic acid (NOTA) complexes.[101] While only used at this time to label small molecules and peptides, this method may be applied in the future to radiolabel NPs. However, issues associated with the high temperature, organic solvent and low pH needed for radiolabelling may preclude widespread adoption. As previously described, phenols can be radioiodinated utilizing iodogen or chloroamine-T as catalysts. Phenols are available in Bolton–Hunter reagent[61] and tyrosines in peptides[17]—both of which have been connected to nanostructures as a common iodination strategy (Figure 3).

Stable co-ordination chemistry is a pre-requisite for accurate *in vivo* use of probes modified with PET radiometals. Chelation is often achieved utilizing a two-step procedure in which chelators are first conjugated onto the NP surface and then subsequently radiolabelled. DOTA has been widely used to label NPs because it is capable of stably binding various metals, and bifunctional

Table 2. Positron emitters for nanoparticle imaging applications

| Isotope | Half-life and most abundant energies (MeV) (% abundance) | Radiolabelling methods | Radiolabelled NPs |
|---|---|---|---|
| $^{13}$N | 9.96 min<br>$\beta^+$: 1.19 (99%)<br>$\varepsilon$: 2.22 (0.182%) | Radioactive activation | $Al_2O_3$ |
| $^{11}$C | 20.36 min<br>$\beta^+$: 0.960 (99%) | Methyl iodine substitution | IONPs |
| $^{18}$F-FDG | 109.8 min<br>$\beta^+$: 0.635 (100%) | Cu catalysed click chemistry between 2-[$^{18}$F]-fluoroethyl azide and alkyne-NHS spacer<br>Michael addition of SiFASH spacer<br>Direct encapsulation of $^{18}$F-FDG | Dendrimers<br>AuNPs<br>$^{18}$F FDG-liposomes |
| $^{76}$Br | 16.0 h<br>$\beta^+$: 3.980 (26%)<br>$\gamma$: 0.559 (74%); 0.657 (16%); 1.854 (15%)[93] | Nucleophilic substitution on tyrosine | Dendrimers |
| $^{124}$I | 100.2 h<br>$\varepsilon/\beta-$: 1.54 (11.7%); 2.14 (10.8%)<br>$\gamma$: 0.603 (63%); 1.691 (10.9%); 0.723 (10.4%)[94] | Nucleophilic substitution on tyrosine catalysed by iodogen | Dendrimers<br>Silica dots |
| $^{68}$Ga | 67.71 min<br>$\beta^+$: 1.899 (89%)<br>$\gamma$: 1.077 (100%) | NOTA chelation<br>Direct radiolabelling | AuNPs<br>IONPs |
| $^{64}$Cu | 12.70 h<br>$\varepsilon/\beta^-$: 0.578 (37%)<br>$\beta^+$: 0.651 (18%)<br>$\gamma$: 0.511 (36%); 0.007–0.008 (34%) | DOTA<br>TETA<br>BAT<br>$DO_3A$ chelation<br>Bisphosphonate<br>Direct radiolabelling | Liposomes; QDs; AuNPs<br>Polymeric micelles<br>Solid lipid NPs<br>QDs<br>IONPs<br>IONPs; AuNPs |
| $^{89}$Zr | 78.4 h<br>$\varepsilon/\beta^+$: 0.897 (77%; 22.6%)<br>$\gamma$: 0.909 (99.9%)[95] | Direct radiolabelling<br>DFO chelation | Liposomes; IONPs<br>IONPs; AuNPs; SWCNTs |
| $^{86}$Y | 14.74 h<br>$\varepsilon/\beta^-$: 1.2 (11.9%); 1.5 (5.6%)<br>$\gamma$: 177 (83%); 0.627 (32.6%); 1.153 (30.5%)[96] | DOTA | SWCNTs |

$\varepsilon$, electron capture; β−, beta decay; β+, positron; AuNPs, gold NPs; IONPs, iron oxide NPs; QDs, quantum dots.

reactive DOTA is commercially available.[102] $^{64}$Cu-DOTA in particular has been widely utilized to visualize NP distribution, including for liposomes,[103,104] AuNPs[105] and IONPs.[106] However, DOTA appears to be an unstable chelator for $^{64}$Cu[107] and also requires heating to gain efficient labelling yield. Subsequent advances have seen NPs prepared with TETA;[23] $DO_3A$[108] or other innovative ligands such as BAT[58] and bisphosphonates[109] resulting in more stable radiocomplexes (Figure 2).

The recent improvement in methods to produce, purify and label $^{89}$Zr to monoclonal antibodies for pre- and clinical investigation has made this radiometal of particular interest for the NP community. The half-life of 3.8 days is well suited to the aforementioned immunoglobulins, as well as longer circulating NPs. The desferioxamine (DFO) chelator has been described as the ligand of choice for immuno-PET imaging (Figure 2). However, recent developments have opened a debate whether DFO is sufficiently stable for $^{89}$Zr use *in vivo*,[110] and alternative chelate design is an active area of research.[111] In addition, direct radiolabelling of NPs using chelator-free approaches have also been investigated with liposomes,[6] silica[112] and IONPs.[113]

## Pre-clinical development overview/role in drug development

### *$^{13}$N, $^{11}$C, $^{18}$F and radiohalogens covalent radiolabelling to nanoparticles*

Rapid radiolabelling of $Al_2O_3$ NPs was reported utilizing an elegant method of NP radioactive activation generating $^{13}$N-enriched NP. This approach enabled immediate characterization of NP PKs comparing various NPs size (from 10 nm to 10 μm diameter). This study showed that the smaller the NPs, the higher the chance of urinary excretion with significant bladder uptake. Increasing particle size resulted in accumulation in liver, spleen and lungs.[114]

To the best of our knowledge, the only report of $^{11}$C-labelling of NPs has been accomplished by $^{11}$C-methylation of IONPs allowing for immediate PK determination. Minutes-long half-life of $^{11}$C limits its use for extended radioactive monitoring. However, further visualization of these particles was defined

utilizing the particles' intrinsic MR contrast. It should be stated however, that the short-lived isotope has the advantage of limiting prolonged radioactive exposure.[41]

Radioactive fluorination has been undertaken on many NP species. Direct fluorination can be employed when working with aluminium oxide or hydroxyapatite NPs. This radiolabelling process is based upon $^{18}$F exchange with hydroxides carried by aluminium oxides or hydroxyapatites. *In vitro* serum assays demonstrated high stability, however, evaluation in mice showed increasing bone uptake owing to defluorination, after predominant lung and liver uptake.[100]

Liposomes have been fluorinated using a variety of strategies. Incorporation of readily made radioactive constructs in formulation is perhaps the most straightforward. Reports of $^{18}$F-FDG and radiofluorinated drugs encapsulated in vesicles showed enhanced drug delivery and enabled imaging of liposomes.[115,116] However, radiation exposure during liposome extrusion and low encapsulation efficiency are the areas of concern. Fluorination of the lipid constituents used to produce the liposomes can be labelled with improved overall efficiency, but similarly, radiation exposure remains a challenge.[98] Alternatively, Urakami et al have proposed $^{18}$F-radiolabelling utilizing preformed liposomes. Single chain lipid constructs were radiofluorinated by tosyl substitution and subsequently incubated with preformed liposomes. This approach resulted in high incorporation efficiency (>80%) and fair *in vitro* stability in serum proteins.[117]

$^{18}$F-radiolabelling of AuNPs has been accomplished exploiting the thiol reactivity of Au-surface. Maleimide functionalized PEG grafted to AuNPs were reacted with thiol substituted $^{18}$F-silicon prosthetic group (Si-FA-SH) through [1,4]-Michael addition. The silicon fluoride construct was produced by fast $^{18}$F isotopic exchange with a t-butyl silicon construct.[99] The resulting carboxylated AuNPs of <3 nm diameter were administered to rats and exhibited transport across the blood brain barrier.[118] A similar process to radiolabel preformed particles has been employed with Cu-catalysed click chemistry to image dendrimers. A succinimidyl alkyne construct was assembled to react with $^{18}$F-fluorinated azide prosthetic group. Amine-terminated generation-6 dendrimers were then conjugated with $^{18}$F-labelled spacer resulting in fast and efficient radiolabelling.[119]

Use of halogen radioisotopes has been explored as well for dendrimers radiolabelling. Dendrimers have been modified with tyrosine allowing for radiohalogen substitution with $^{125}$I or $^{76}$Br. Tyrosine amines were attached to RGD for specific angiogenesis imaging application.[120] Similarly, Benezra et al[121] utilized RGD tyrosine as a site for iodination of silica dots for $^{124}$I-PET imaging of human melanoma.

### *Co-ordination chemistry and electrostatic interaction for nanoparticle radiolabelling*

Positron emitting radiometals including $^{68}$Ga, $^{64}$Cu, $^{86}$Y and $^{89}$Zr can be bound to NPs by electrostatic interactions or co-ordination chemistry. Generally, $^{68}$Ga is used to probe short biological phenomena, while $^{64}$Cu, $^{86}$Y and $^{89}$Zr enable longer investigation and identification of NP body residency time.

Various AuNP surface chemistries and sizes have been compared to investigate short-term PKs using a $^{68}$Ga-NOTA radiolabelling approach. NOTA was conjugated using a long or short arms to glycopeptide-functionalized AuNPs and subsequently radiolabelled by mixing with $^{68}$Ga.[122] Short spacer conjugation and peptide modification exhibited an increased renal clearance as compared with other formulations. Furthermore, this preparation enabled a higher brain uptake, showing the potential of AuNPs for neuroimaging. AuNPs were also radiolabelled utilizing $^{64}$Cu-DOTA to provide a long-term investigation of distribution out to 44 h p.i.[105,123] Grafting AuNPs with 2K and longer PEG chains significantly increased NP diameter (to 20–50 nm) resulting in enhanced liver and spleen uptake.[123]

Direct incorporation of the radiolabel within the nanostructure can also be conducted. Human serum albumin-stabilized gold nanoclusters were doped with $^{64}$Cu to generate dual-modality near infrared (NIR) fluorescence and PET-capable ultrasmall particles (7 nm), which were then characterized *in vivo*. Tumour targeting was achieved with 15% IA/g 24 h p.i. but notable liver uptake (up to 30% IA/g) was noticed as early as 1 h p.i.[124] AuNPs have been tracked through conjugation of $^{89}$Zr-radiolabed mAb. $^{89}$Zr-tracking enables visualization up to 168 h p.i.[125,126]

Liposomes exhibit long *in vivo* circulation, especially when grafted with PEG chains.[127] For accurate characterization, they require stable radiochemical modification, with long radioisotopes. PET imaging of liposomes has therefore been undertaken utilizing $^{64}$Cu and $^{89}$Zr. Similar to SPECT radiolabelling, loading radionuclides into the aqueous compartment of the particles has been tested. Here, liposomes were formulated with encapsulated DOTA to enable $^{64}$Cu incorporation by using the lipophilic transporter hydroxyquinoline. These $^{64}$Cu-liposomes have then been used for both tumour and inflammation imaging.[128,129] Direct $^{64}$Cu-radiolabelling of the liposomal surface has been achieved using with BAT, a stable chelator of $^{64}$Cu.[130] The chelator was conjugated to the end of PEG chains and radiolabelling was conducted on preformed NPs. $^{64}$Cu has enabled extended visualization of NPs up to approximately 48 h p.i.

For longer imaging, $^{89}$Zr-labelling has been used.[131] $^{89}$Zr-radiolabelling of liposomes was conducted utilizing DFO chelation of PEG-functionalized lipids[131] or by direct embedment in lipid membranes.[6] The latter provides a straightforward approach with minimal modification but produces moderately stable particles, with significant bone uptake as compared with DFO-conjugated liposomes. Tumour-targeted PET liposomes have been synthesized by conjugation to octreotide[6] or octreotate[103] (the C-terminal threonine in octreotide being replaced with threonine to yield octreotate). These peptides target a subset of the somatostatin receptors (sstr2), which is overexpressed on neuroendocrine tumour cells.[132] Although octreotate receptor affinity for the sstr2 receptor is known to be higher than DOTA-[Tyr3] octreotide (IC50 = 1.5 *vs* 14 nM, respectively[132]), octreotate-liposomes did not show greater tumour-specific contrast in comparison with octreotide-liposomes. Peptide-conjugated liposomes resulted in higher liver and spleen uptake as compared with control PEG-liposomes, a result of increased RES filtration. In additional to liposomal approaches, polymer-based particles

have been closely investigated. Micelles made of block co-polymers were engineered and radiolabelled with $^{64}$Cu-TETA. Folate bound to the end of $PEG_{1.6K}$ chains were conjugated to NPs. The majority of uptake was revealed in the lungs, liver and spleen as early as 10 min p.i. Tumour targeting was, however, not achieved when compared with controls.[23] Taken together, these results raise interesting question about the overall ability of targeting ligands to direct (relatively) large NPs structures to disease sites through active uptake mechanisms.

In the absence of targeting ligands, PET radiolabelling has afforded the ability to image the effect of surface coating for NP distribution. Here, $^{64}$Cu-DOTA-labelled CdSe QD-$PEG_{2000}$ was compared to similarly radiolabelled non-coated QDs. Delayed uptake in the liver and spleen was noted when QDs were PEG-shielded.[11] Smaller-sized InAs QDs have also been investigated with PEG shielding and peptide modification, which demonstrate increased renal clearance when peptides were conjugated, while blood circulation was extended when PEG coated.[133]

Dextran-formulated polysaccharide NPs have been radiolabelled with $^{89}$Zr-DFO to track macrophages.[134] The sugar polymer, synthesized into spherical nanostructures, was modified for amino functionalization, providing a site for conjugation of fluorescent probes and $^{89}$Zr-radiolabelling with DFO. This labelling strategy was used to investigate the effect of size and functionalization of dextran NPs *in vivo*, where it was noted that the smaller the size, the faster the clearance from blood. Similarly, the more hydrophilic the coating, the faster the blood clearance. Little uptake was noted in background organs, as NPs distributed mostly into lymph nodes, liver and spleen. The tracking of tumour-associated macrophage was further confirmed by fluorescence flow cytometry of digested tumour tissues.

Covalently functionalized, single-walled CNTs have also been evaluated using PET radiometals. CNTs were conjugated with DOTA for $^{86}$Y labelling[19] or with DFO for $^{89}$Zr labelling.[135] These strategies have provided insight into both the short and long-term distribution characteristics of these NPs. Surprisingly for their long length, renal excretion was the major pathway of CNT clearance. Furthermore, fluorescent tagging of the same particles enabled investigators to focus on the uptake mechanism in renal tubule cells. This radiosensitive cell is relevant for radiotherapy applications utilizing an α-particle emitting $^{225}$Ac-CNT construct evaluated to treat a colon cancer model.[135] It was demonstrated that CNTs were located on the basal compartment of the kidney cells, enabling use of this potent therapy with minimally observed toxic effect.

### Translation of nanoparticles for positron emission tomography imaging

To date, few PET-radiolabelled NPs have been evaluated clinically. C-dots are perhaps the pioneer PET-labelled NPs and are currently undergoing translation in Phase I clinical trial to evaluate safety and efficiency (ClinicalTrials.gov identifier: NCT01266096) (Figure 4). C-dots are constituted of an inorganic core with a Cy5.5-fluorescent dye, stabilized by a silica shell. The formulation used in clinical investigation is PEG coating to avoid RES uptake and modified with a $^{124}$I-labelled-cRGD peptide for tumour-targeting to the $\alpha_v\beta_3$-integrin, expressed on malignant neovasculature.[121] At this time, evaluation of the compound in five patients with melanoma and some with malignant brain tumours have been published.[17] Whole body patient imaging demonstrated uptake in the gallbladder, heart, intestines and bladder as well as localization to the tumour (Figure 4).

The *in vivo* residency time in humans displayed both immediate- and delayed-clearance phases with measured values of $t_{1/2}$ (1) = 3.75 h and $t_{1/2}$ (2) = 48 h, respectively. The mechanism of clearance was through the kidney, which produces the advantage of fully removing the particles (rather than, for example, decomposition in the liver).[16] Complete PKs, organ dosimetry and follow-up of NP metabolites in plasma and urine were evaluated. Ultimately, this multimodality imaging NP platform may facilitate tumour detection utilizing PET and ease tumour resection utilizing fluorescent-guided surgery. Furthermore, the initial evaluation of the agent in patients with melanoma is being expanded to guided lymph node imaging in patients with head and neck, melanoma, prostate and cervical cancer (ClinicalTrials.gov identifier: NCT02106598). This trial focuses on utilizing a single nanostructure for two or more imaging modalities, which will be explored in the following section.

## MULTIMODAL IMAGING WITH RADIOLABELLED NANOPARTICLES

With the emergence of multimodality imaging scanners such as PET, SPECT/CT and PET/MR, also came pre-clinical developments in the form of probes. Considering the variety and customization of NP compositions and their diversity in surface chemistries, nanostructures are ideal platforms for multimodality imaging application.

A major driving force for the development of NP-based imaging agents and more broadly for the application of NPs in biomedical science is the potential for multiplexing. As the synthesis, modification and characterization of NPs has improved in the past two decades, intense effort has been focused on their use as multifunctional platforms. Specifically for diagnostic and disease monitoring applications, signal generation in more than one imaging modality is of use to take advantage of the strengths of each modality. CT and MR provide important anatomical detail, emerging optical imaging technologies generate high resolution and post-mortem histological verification, while PET and SPECT enable high sensitivity of detection of metabolism and ligand-targeted information. Taken individually, each modality presents its own advantages and limitations. Combining two or three imaging modalities within the same NP formulation allows for the exploitation of each modality's advantageous properties.

By virtue of the physical properties of their constituents IONPs, AuNPs and QDs feature original imaging contrasts for MR, CT or optical imaging, respectively. NP radiolabelling opens a route towards novel diagnostic approaches utilizing simultaneous contrasts in multiple modalities. An attractive prospective of multimodality imaging utilizing NPs is the application for image-guided surgery facilitating sensitive deep tissue detection of disease by PET, followed by precise tissue resection by optical contrast.[17,136]

Figure 4. Whole-body positron emission tomography (PET)-CT imaging of $^{124}$I-cRGDY–polyethylene glycol–Cornell dots. Intravenous injection of $^{124}$I-cRGDY-PET-C-dots followed by repeat imaging in a Phase I safety and feasibility study (ClinicalTrials.gov identifier NCT01266096). Representative whole-body image of (a) CT, (b) PET at 4 h and (c) PET/CT at 4 h and (d) at 24 h. (e) Corresponding fluorine-18 fludeoxyglucose PET/CT image of hepatic metastasis in (a); (arrow). Colour and grey scales reflect PET standardized uptake value. Reproduced from Phillips et al[17] with permission from American Association for the Advancement of Science.

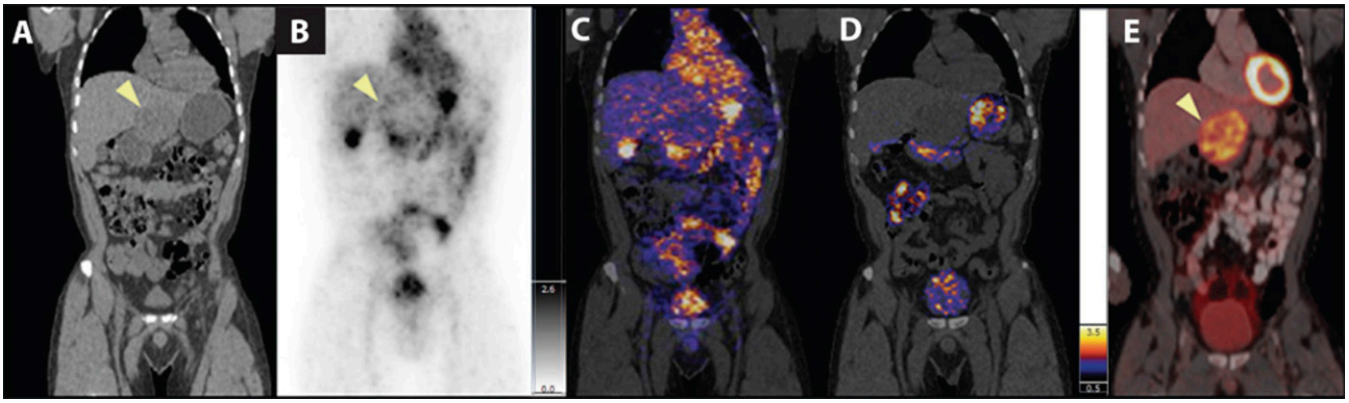


## Positron emission tomography/MR and single photon emission CT/MR nanoparticles

The complementary nature of different imaging methods has been a major force driving improvements in clinical radiology and pre-clinical research. Most notably, the fusions of PET/CT and SPECT/CT have enabled researchers and clinicians to visualize functional and anatomical details simultaneously. The overriding advantage is the exact localization of sites of radiotracer uptake. In the last decade, advances in imaging scanner technology resulted in the emergence of novel devices combining complementary imaging modalities, such as PET/MR and PET-SPECT/CT. PET and SPECT are ultrasensitive, quantitative imaging techniques that determine functional mechanism, whereas CT and MR confer detailed morphological and anatomical information. The development of multimodality imaging probes may be of tremendous benefit for defined medical applications. For example, radiolabelled IONPs may increase the sensitivity of lymph node detection by nuclear imaging, to assist disease detection by anatomical MRI in humans.[137]

Specific radiofrequency (RF) pulse sequences are used in MRI to visualize contrast between adjacent tissues. These RF sequences are designed to accentuate the longitudinal (also known as $T_1$) or transverse ($T_2$) relaxation times of the protons in a particular tissue. Pulse sequences vary the excitation and time of readout in order to capture the $T_1$ and/or $T_2$ signal of a particular tissue. The $T_1$ or $T_2$ signal is dependent on several factors which include proton density and the biochemical nature of the hydrogen atoms present in that organ or liquid. Contrast agents are applied to locally enhance the signal in a given imaging protocol. While all contrast agents possess both $T_1$ and $T_2$ effects, contrast agents are generally characterized by their dominant contrast mode. $T_1$ weighted contrast agents increase the rate at which protons realign with the applied magnetic field (thereby increasing signal locally in $T_1$ weighted imaging). Conversely, $T_2$-contrast agents (such as IONPs) function by enhancing the loss of coherent precession of local protons (thereby decreasing signal locally in $T_2$ weighted imaging). Commonly, iron oxides are referred to as $T_2$* contrast agents, a term that refers to the observed $T_2$ signal, shortened by unavoidable magnetic field inhomogeneities and other field distortions.

Combining PET with $T_1$ weighted Gd-engineered NPs have been prepared with radiolabelled liposomes ($^{89}$Zr, $^{64}$Cu and $^{111}$In) formulated with Gd-DTPA/DOTA-lipids.[6,57,138] Another reported strategy describes inorganic upconversion nanophosphors, incorporating rare earth metals and Gd into a nanostructure. These NPs produce detectable spin-lattice MR contrast enhancement and are radiolabelled with $^{18}$F for dual PET/MRI.[44]

The $T_2$-contrast producing IONP agents have been widely investigated for combined SPECT and PET with MR. These particles may be ferro- or superparamagnetic, enabling contrast in MRI through the production of localized magnetic field inhomogeneities.[139] Formulations of IONPs (free of a radiolabel) have been approved for clinical use and are under investigation for a range of disease detection applications including breast, pancreatic, thyroid and head and neck cancer (ClinicalTrials.gov identifier: NCT02249208; NCT00920023; NCT01885829; NCT01927887). Using these NP platforms, IONPs are an inherent multimodality imaging agent for dual PET/MR ($^{89}$Zr-labelled ferumoxytol[140] or SPECT/MRI ($^{111}$In-labelled IONP,[49] as well as trimodality imaging MR/NIR/PET or SPECT when conjugated to fluorescent near-infrared optical agents (see the Radiolabelled fluorescent nanoparticle section). Radiolabelled IONPs with SPECT imaging isotopes using direct labelling or doping approaches have produced $^{99m}$Tc-labelled and $^{111}$In-incorporating IONPs.[47,49] Alternatively, to preformed particles, $^{99m}$Tc-bisphosphonate can be used to radiolabel IONPs.[141] SPECT and $T_2$-MR, and $^{99m}$Tc-IONPs have demonstrated sensitive identification of lymph nodes in rats.

Fast and efficient click chemistry strategies have also been leveraged to produce $^{18}$F-radiolabelled IONPs. $^{18}$F-labelling was conducted with Huisgen cycloaddition of a fluorinated alkyne to azide-modified NP surfaces.[142] This PET/MRI agent permitted macrophage tracking in aortic aneurysms in mice.[143] IONPs

have also been radiolabelled for PET imaging with radiometals such as $^{68}$Ga (doped),[144] $^{64}$Cu (doped or DOTA/bisphosphonate chelated),[109,145,146] or $^{89}$Zr (doped or DFO chelated).[113,140] The high radioactive concentration per NP, or specific activity, is propitious for Cerenkov imaging, further presented in the last section of this review.[140,144]

### Radiolabelled fluorescent nanoparticles

Combination of nuclear and optical imaging is beneficial considering the complementary advantages of each modality. Nuclear imaging is quantitative, sensitive and does not have any tissue-depth limitation, while optical imaging can be sensitive and is applicable to real-time intraoperative contexts but is only amenable at shallow depth or in exposed tissues.[147] The modalities may therefore be combined to provide a means to simultaneously detect deep tissues, for subsequent guided resection of sites of interest, often lymph nodes or disease foci. Nuclear imaging scans localize the zone to operate, and optical image guidance helps to complete precise resection of tumours or metastases.

Radiolabelled fluorescent NPs demonstrate useful features for histopathological evaluation of diseased tissues. As well, this approach provides a means for high-resolution cellular and subcellular *in vitro* study of NPs interaction with cells by fluorescence microscopy.[148] Some NPs, such as IONP have been conjugated with fluorophores (Cy5; VT680)[149,150] and radiolabelled (with $^{64}$Cu or $^{18}$F) for tracking of macrophages at inflammation sites[150] or for detection of intracardiac macrophages.[143] Other NPs such as QDs have intrinsic fluorescent features,[148,151] that afford fluorescent imaging of the radiolabelled particles. As mentioned above, the C-dot PET NP currently undergoing clinical evaluation encapsulates Cy5.5 fluorophore.[17] It is hoped that this will contribute for multimodal imaging applications using this NP platform to non-invasively detect disease by PET, followed by fluorescence-guided resection.

### Cerenkov radiation imaging with nanoparticles

As an alternative to radiolabelling of NP platforms, which present contrast in other modalities (for example, radiolabelling fluorescent QDs), the radioisotope itself has the potential to enable multimodal nuclear/optical imaging. Cerenkov radiation (CR), named for Dr Pavel Cerenkov's characterization of this phenomenon, is a physical process by which high-energy charged particles produce ultraviolet- and visible-wavelength light when travelling through dialectric media (such as water or tissues).[152,153] Several conditions must be met for the production of this light; most critically sufficient velocity of the charged particle at super-relativistic speeds in the media. In water, with a refractive index of 1.33, the required velocity threshold is 263 keV and is met by many of the $\beta^+$ emitting particles used for PET imaging and radiotherapeutic radionuclides such as $^{90}$Y, $^{131}$I, $^{177}$Lu and $^{225}$Ac.[154]

At this time, applications in CR optical imaging have predominantly used PET isotopes.[155–157] NPs provide a platform to achieve a high number of radionuclides per structure, which may be essential in many CR imaging applications because of the low number of visible photons produced per disintegration.[154] Tyrosine-conjugated polymer-coated IONPs were radioiodinated with iodogen beads and $^{124}$I, to produce a probe for optical/PET/MRI.[158] Following dermal injection in the footpad, lymph nodes can be identified using optical, PET and MRI. Optical/MRI of nodes with the short-lived $^{68}$Ga bound magnetic NPs using a direct labelling method was demonstrated.[144] Systemic imaging of optical/PET/MR liposomes has also been achieved, using a radioiodinated ($^{124}$I) lipid analogue constituent.[159] $\gamma$ emitting $^{198}$Au (clinically used as a colloid for local treatment of arthritis[160] and meningosis[161]) has been labelled to AuNPs of controlled shapes and subsequently optically imaged by CR emissions[162] and evaluated to treat a breast cancer model in mice.

While nuclear imaging provides exquisite sensitivity unmatched for deep tissue whole-body molecular imaging, the physical principles of PET preclude imaging of multiple tracers simultaneously (as is commonly done with fluorescent agents) or the construction of activatable contrast agents. Such activatable probes respond to molecular or cellular events to enable readout of physiological or disease processes. CR allows for both multispectral and activatable nuclear probes to be evaluated. As recently investigated, implicated enzymatic activity was visualized in aggressive disease of a breast cancer model.[163] Here, AuNPs were conjugated to a fluorophore via an enzyme-cleavable linker. When bound to the particle, the fluorescence of the fluorophore is quenched, but after cleavage can be excited by CR and the fluorescence spectrally distinguished. A similar distance-dependent activatable strategy has utilized $^{64}$Cu-conjugated DNA sequences of varying length bound to QD. Distance-dependent spectral shifting of the CR via the fluorescent QD was noted.[164]

In an alternative strategy, the Cerenkov signal can be quenched by absorbing NPs. For example, NPs can be directed to sites of disease, which are concomitantly targeted with $^{18}$F-FDG. In the event of co-localization, the CR signal is diminished, enabling combined optical and nuclear imaging to enhance the information content from a single study.[165]

The continuous spectrum of light produced by the CR effect is weighted to the short wavelength UV and blue. NIR fluorescent NPs coupled to CR-producing radioisotopes absorb the blue light of the CR and emit red-shifted fluorescent light. Red and NIR light can travel deeper through tissue for more efficient detection. QDs have been mixed with radionuclides for this effect, which also enables multiplexing (spectral distinction of different probes simultaneously).[153,163,166,167]

## CONCLUSIONS AND FUTURE DIRECTIONS

Biomaterial and chemical engineering developments have created opportunities for multifunctionalized NP platforms across many scientific disciplines. The significant medical potential of these NPs has generated intense interest in the molecular imaging and radiology communities. Careful construction and evaluation of these NP probes using nuclear imaging methods provides considerable insight into their *in vivo* fate and their prospective utility in research and clinical application. These discoveries have demonstrated how size, charge, shape and surface chemistry are critical criteria to consider for NP biocompatibility, safety and clearance. Ultimately, few nanoformulations have made

it to the evaluation stage in man. However, there are several NP platforms in the planning stages of translation, bolstered by the demonstrated feasibility and safety of the $^{124}$I-labelled C-dot technology. Applied in patients with melanoma and malignant brain tumours, detailed PK and diagnostic parameters have readily been assessed.

Radiolabelled NPs have been investigated for single-modality SPECT and PET imaging, as well as multimodality nuclear MR and optical imaging in a range of pre-clinical models. These accomplishments may open new paths and technical developments for the ultimate goal of facilitating diagnosis of disease and precise medicine.[92,96]

## REFERENCES


1. Kolhar P, Anselmo AC, Gupta V, Pant K, Prabhakarpandian B, Ruoslahti E, et al. Using shape effects to target antibody-coated nanoparticles to lung and brain endothelium. *Proc Natl Acad Sci U S A* 2013; **110**: 10753–8. doi: 10.1073/pnas.1308345110
2. Longmire M, Choyke PL, Kobayashi H. Clearance properties of nano-sized particles and molecules as imaging agents: considerations and caveats. *Nanomedicine (Lond)* 2008; **3**: 703–17. doi: 10.2217/17435889.3.5.703
3. Maeda H, Wu J, Sawa T, Matsumura Y, Hori K. Tumor vascular permeability and the EPR effect in macromolecular therapeutics: a review. *J Control Release* 2000; **65**: 271–84. doi: 10.1016/S0168-3659(99)00248-5
4. Bangham AD. Lipid bilayers and biomembranes. *Annu Rev Biochem* 1972; **41**: 753–76. doi: 10.1146/annurev.bi.41.070172.003541
5. Laverman P, Brouwers AH, Dams ET, Oyen WJ, Storm G, van Rooijen N, et al. Preclinical and clinical evidence for disappearance of long-circulating characteristics of polyethylene glycol liposomes at low lipid dose. *J Pharmacol Exp Ther* 2000; **293**: 996–1001.
6. Abou DS, Thorek DL, Ramos NN, Pinkse MW, Wolterbeek HT, Carlin SD, et al. (89)Zr-labeled paramagnetic octreotide-liposomes for PET-MR imaging of cancer. *Pharm Res* 2013; **30**: 878–88. doi: 10.1007/s11095-012-0929-8
7. Cai W, Hong H. In a "nutshell": intrinsically radio-labeled quantum dots. *Am J Nucl Med Mol Imaging* 2012; **2**: 136–40.
8. Michalet X, Pinaud FF, Bentolila LA, Tsay JM, Doose S, Li JJ, et al. Quantum dots for live cells, *in vivo* imaging, and diagnostics. *Science* 2005; **307**: 538–44. doi: 10.1126/science.1104274
9. Barar J, Omidi Y. Surface modified multifunctional nanomedicines for simultaneous imaging and therapy of cancer. *Bioimpacts* 2014; **4**: 3–14. doi: 10.5681/bi.2014.011
10. Choi HS, Frangioni JV. Nanoparticles for biomedical imaging: fundamentals of clinical translation. *Mol Imaging* 2010; **9**: 291–310.
11. Schipper ML, Cheng Z, Lee SW, Bentolila LA, Iyer G, Rao J, et al. microPET-based biodistribution of quantum dots in living mice. *J Nucl Med* 2007; **48**: 1511–18. doi: 10.2967/jnumed.107.040071
12. Pinaud F, King D, Moore HP, Weiss S. Bioactivation and cell targeting of semiconductor CdSe/ZnS nanocrystals with phytochelatin-related peptides. *J Am Chem Soc* 2004; **126**: 6115–23. doi: 10.1021/ja031691c
13. Ow H, Larson DR, Srivastava M, Baird BA, Webb WW, Wiesner U. Bright and stable core-shell fluorescent silica nanoparticles. *Nano Lett* 2005; **5**: 113–17. doi: 10.1021/nl0482478
14. Larson DR, Ow H, Vishwasrao HD, Heikal AA, Wiesner U, Webb WW. Silica nanoparticle architecture determines radiative properties of encapsulated fluorophores. *Chem Mater* 2008; **20**: 2677–84. doi: 10.1021/cm7026866
15. Choi HS, Liu W, Misra P, Tanaka E, Zimmer JP, Itty Ipe B, et al. Renal clearance of quantum dots. *Nat Biotechnol* 2007; **25**: 1165–70. doi: 10.1038/nbt1340
16. Burns AA, Vider J, Ow H, Herz E, Penate-Medina O, Baumgart M, et al. Fluorescent silica nanoparticles with efficient urinary excretion for nanomedicine. *Nano Lett* 2009; **9**: 442–8. doi: 10.1021/nl803405h
17. Phillips E, Penate-Medina O, Zanzonico PB, Carvajal RD, Mohan P, Ye Y, et al. Clinical translation of an ultrasmall inorganic optical-PET imaging nanoparticle probe. *Sci Transl Med* 2014; **6**: 260ra149. doi: 10.1126/scitranslmed.3009524
18. Kostarelos K, Bianco A, Prato M. Promises, facts and challenges for carbon nanotubes in imaging and therapeutics. *Nat Nanotechnol* 2009; **4**: 627–33. doi: 10.1038/nnano.2009.241
19. Ruggiero A, Villa CH, Bander E, Rey DA, Bergkvist M, Batt CA, et al. Paradoxical glomerular filtration of carbon nanotubes. *Proc Natl Acad Sci U S A* 2010; **107**: 12369–74. doi: 10.1073/pnas.0913667107
20. Lacerda L, Ali-Boucetta H, Herrero MA, Pastorin G, Bianco A, Prato M, et al. Tissue histology and physiology following intravenous administration of different types of functionalized multiwalled carbon nanotubes. *Nanomedicine (Lond)* 2008; **3**: 149–61. doi: 10.2217/17435889.3.2.149
21. Denkova AG, Mendes E, Coppens MO. Kinetics and mechanism of the sphere-to-rod transition of triblock copolymer micelles in aqueous solutions. *J Phys Chem B* 2009; **113**: 989–96. doi: 10.1021/jp807513k
22. Wang G, de Kruijff R, Stuart MCA, Mendes E, Wolterbeek HT, Denkova AG. Polymersomes as radionuclide carriers loaded via active ion transport through the hydrophobic bilayer. *Soft Matter* 2013; **9**: 727–34. doi: 10.1039/C2SM26434J
23. Rossin R, Pan D, Qi K, Turner JL, Sun X, Wooley KL, et al. 64Cu-labeled folate-conjugated shell cross-linked nanoparticles for tumor imaging and radiotherapy: synthesis, radiolabeling, and biologic evaluation. *J Nucl Med* 2005; **46**: 1210–18.
24. Tomalia DA, Naylor AM, Goddard WA. Starburst dendrimers: molecular-level control of size, shape, surface-chemistry, topology, and flexibility from atoms to macroscopic matter. *Angew Chem Int Ed Engl* 1990; **29**: 138–75. doi: 10.1002/anie.199001381
25. Frechet JM. Functional polymers and dendrimers: reactivity, molecular architecture, and interfacial energy. *Science* 1994; **263**: 1710–15. doi: 10.1126/science.8134834
26. Wu CC, Brechbiel MW, Kozak RW, Gansow OA. Metal-chelate-dendrimer-antibody constructs for use in radioimmunotherapy and imaging. *Bioorg Med Chem Lett* 1994; **4**: 449–54. doi: 10.1016/0960-894X(94)80014-6
27. Daniel MC, Astruc D. Gold nanoparticles: assembly, supramolecular chemistry, quantum-size-related properties, and applications toward biology, catalysis, and nanotechnology. *Chem Rev* 2004; **104**: 293–346. doi: 10.1021/cr030698+
28. Giljohann DA, Seferos DS, Daniel WL, Massich MD, Patel PC, Mirkin CA. Gold

nanoparticles for biology and medicine. *Angew Chem Int Ed Engl* 2010; **49**: 3280–94. doi: 10.1002/anie.200904359
29. Akerman ME, Chan WC, Laakkonen P, Bhatia SN, Ruoslahti E. Nanocrystal targeting *in vivo*. *Proc Natl Acad Sci U S A* 2002; **99**: 12617–21. doi: 10.1073/pnas.152463399
30. Ray PC, Fortner A, Darbha GK. Gold nanoparticle based FRET assay for the detection of DNA cleavage. *J Phys Chem B* 2006; **110**: 20745–8. doi: 10.1021/jp065121l
31. Bastus NG, Sanchez-Tillo E, Pujals S, Farrera C, Lopez C, Giralt E, et al. Homogeneous conjugation of peptides onto gold nanoparticles enhances macrophage response. *ACS Nano* 2009; **3**: 1335–44. doi: 10.1021/nn8008273
32. Conde J, Bao C, Cui D, Baptista PV, Tian F. Antibody-drug gold nanoantennas with Raman spectroscopic fingerprints for *in vivo* tumour theranostics. *J Control Release* 2014; **183**: 87–93. doi: 10.1016/j.jconrel.2014.03.045
33. Cao YC, Jin R, Thaxton CS, Mirkin CA. A two-color-change, nanoparticle-based method for DNA detection. *Talanta* 2005; **67**: 449–55. doi: 10.1016/j.talanta.2005.06.063
34. Chen K, Xie J, Chen X. RGD-human serum albumin conjugates as efficient tumor targeting probes. *Mol Imaging* 2009; **8**: 65–73.
35. Josephson L, Tung CH, Moore A, Weissleder R. High-efficiency intracellular magnetic labeling with novel superparamagnetic-Tat peptide conjugates. *Bioconjug Chem* 1999; **10**: 186–91. doi: 10.1021/bc980125h
36. Pala A, Liberatore M, D'Elia P, Nepi F, Megna V, Mastantuono M, et al. Labelling of granulocytes by phagocytic engulfment with 64Cu-labelled chitosan-coated magnetic nanoparticles. *Mol Imaging Biol* 2012; **14**: 593–8. doi: 10.1007/s11307-011-0526-y
37. Wunderbaldinger P, Josephson L, Weissleder R. Crosslinked iron oxides (CLIO): a new platform for the development of targeted MR contrast agents. *Acad Radiol* 2002; **9** (Suppl. 2): S304–6.
38. Zolata H, Abbasi Davani F, Afarideh H. Synthesis, characterization and theranostic evaluation of Indium-111 labeled multifunctional superparamagnetic iron oxide nanoparticles. *Nucl Med Biol* 2015; **42**: 164–70. doi: 10.1016/j.nucmedbio.2014.09.007
39. Lewin M, Carlesso N, Tung CH, Tang XW, Cory D, Scadden DT, et al. Tat peptide-derivatized magnetic nanoparticles allow *in vivo* tracking and recovery of progenitor cells. *Nat Biotechnol* 2000; **18**: 410–14. doi: 10.1038/74464
40. Chrastina A, Schnitzer JE. Iodine-125 radiolabeling of silver nanoparticles for *in vivo* SPECT imaging. *Int J Nanomedicine* 2010; **5**: 653–9. doi: 10.2147/IJN.S11677
41. Sharma R, Xu Y, Kim SW, Schueller MJ, Alexoff D, Smith SD, et al. Carbon-11 radiolabeling of iron-oxide nanoparticles for dual-modality PET/MR imaging. *Nanoscale*. 2013; **5**: 7476–83. doi: 10.1039/c3nr02519e
42. Wang C, Tang F, Wang X, Li L. Self-assembly of fluorescent hybrid core-shell nanoparticles and their application. *ACS Appl Mater Interfaces* 2015; **7**: 13653–8. doi: 10.1021/acsami.5b03440
43. Yin S, Li Z, Cheng L, Wang C, Liu Y, Chen Q, et al. Magnetic PEGylated Pt3Co nanoparticles as a novel MR contrast agent: *in vivo* MR imaging and long-term toxicity study. *Nanoscale* 2013; **5**: 12464–73. doi: 10.1039/c3nr04212j
44. Liu Q, Sun Y, Li C, Zhou J, Li C, Yang T, et al. 18F-Labeled magnetic-upconversion nanophosphors via rare-Earth cation-assisted ligand assembly. *ACS Nano* 2011; **5**: 3146–57. doi: 10.1021/nn200298y
45. Fanti S, Farsad M, Mansi L. *Atlas of SPECT-CT*. Berlin, Germany: Springer; 2011. xi. pp. 229.
46. Du Y, Frey EC. Quantitative evaluation of simultaneous reconstruction with model-based crosstalk compensation for 99mTc/123I dual-isotope simultaneous acquisition brain SPECT. *Med Phys* 2009; **36**: 2021–33. doi: 10.1118/1.3120411
47. Madru R, Kjellman P, Olsson F, Wingardh K, Ingvar C, Stahlberg F, et al. 99mTc-labeled superparamagnetic iron oxide nanoparticles for multimodality SPECT/MRI of sentinel lymph nodes. *J Nucl Med* 2012; **53**: 459–63. doi: 10.2967/jnumed.111.092437
48. Psimadas D, Baldi G, Ravagli C, Bouziotis P, Xanthopoulos S, Franchini MC, et al. Preliminary evaluation of a 99mTc labeled hybrid nanoparticle bearing a cobalt ferrite core: *in vivo* biodistribution. *J Biomed Nanotechnol* 2012; **8**: 575–85. doi: 10.1166/jbn.2012.1412
49. Zeng J, Jia B, Qiao R, Wang C, Jing L, Wang F, et al. *In situ* 111In-doping for achieving biocompatible and non-leachable 111In-labeled Fe3O4 nanoparticles. *Chem Commun (Camb)* 2014; **50**: 2170–2. doi: 10.1039/c3cc48948e
50. Steigman J, Solomon NA, Hwang LL. Technetium-sulfur colloid. *Int J Rad Appl Instrum* 1986; **37**: 223–9. doi: 10.1016/0883-2889(86)90175-9
51. Holl G, Dorn R, Wengenmair H, Weckermann D, Sciuk J. Validation of sentinel lymph node dissection in prostate cancer: experience in more than 2,000 patients. *Eur J Nucl Med Mol Imaging* 2009; **36**: 1377–82. doi: 10.1007/s00259-009-1157-2
52. Hung JC, Wiseman GA, Wahner HW, Mullan BP, Taggart TR, Dunn WL. Filtered technetium-99m-sulfur colloid evaluated for lymphoscintigraphy. *J Nucl Med* 1995; **36**: 1895–901.
53. Richardson VJ, Jeyasingh K, Jewkes RF, Ryman BE, Tattersall MH. Properties of [99mTc] technetium-labelled liposomes in normal and tumour-bearing rats. *Biochem Soc Trans* 1977; **5**: 290–1.
54. Goins B, Klipper R, Rudolph AS, Cliff RO, Blumhardt R, Phillips WT. Biodistribution and imaging studies of technetium-99m-labeled liposomes in rats with focal infection. *J Nucl Med* 1993; **34**: 2160–8.
55. Goto R, Kubo H, Okada S. Liposomes prepared from synthetic amphiphiles. I. Their technetium labeling and stability. *Chem Pharm Bull (Tokyo)* 1989; **37**: 1351–4.
56. Laverman P, Dams ET, Oyen WJ, Storm G, Koenders EB, Prevost R, et al. A novel method to label liposomes with 99mTc by the hydrazino nicotinyl derivative. *J Nucl Med* 1999; **40**: 192–7.
57. Mitchell N, Kalber TL, Cooper MS, Sunassee K, Chalker SL, Shaw KP, et al. Incorporation of paramagnetic, fluorescent and PET/SPECT contrast agents into liposomes for multimodal imaging. *Biomaterials* 2013; **34**: 1179–92. doi: 10.1016/j.biomaterials.2012.09.070
58. Andreozzi E, Seo JW, Ferrara K, Louie A. Novel method to label solid lipid nanoparticles with 64cu for positron emission tomography imaging. *Bioconjug Chem* 2011; **22**: 808–18. doi: 10.1021/bc100478k
59. Harrington KJ, Mohammadtaghi S, Uster PS, Glass D, Peters AM, Vile RG, et al. Effective targeting of solid tumours in patients with locally advanced cancers by radiolabeled pegylated liposomes. *Clin Cancer Res* 2001; **7**: 243–54.
60. Black KC, Akers WJ, Sudlow G, Xu B, Laforest R, Achilefu S. Dual-radiolabeled nanoparticle SPECT probes for bioimaging. *Nanoscale* 2015; **7**: 440–4. doi: 10.1039/c4nr05269b
61. Park JJ, Lee TS, Kang JH, Song R, Cheon GJ. Radioiodination and biodistribution of quantum dots using Bolton-Hunter reagent. *Appl Radiat Isot* 2011; **69**: 56–62. doi: 10.1016/j.apradiso.2010.09.004
62. Proffitt RT, Williams LE, Presant CA, Tin GW, Uliana JA, Gamble RC, et al. Tumor-imaging potential of liposomes loaded with

In-111-NTA: biodistribution in mice. *J Nucl Med* 1983; **24**: 45–51.
63. Ogawa M, Umeda IO, Kosugi M, Kawai A, Hamaya Y, Takashima M, et al. Development of 111In-labeled liposomes for vulnerable atherosclerotic plaque imaging. *J Nucl Med* 2014; **55**: 115–20. doi: 10.2967/jnumed.113.123158
64. Boerman OC, Storm G, Oyen WJ, van Bloois L, van der Meer JW, Claessens RA, et al. Sterically stabilized liposomes labeled with indium-111 to image focal infection. *J Nucl Med* 1995; **36**: 1639–44.
65. Awasthi V, Goins B, McManus L, Klipper R, Phillipsa WT. [99mTc] liposomes for localizing experimental colitis in a rabbit model. *Nucl Med Biol* 2003; **30**: 159–68. doi: 10.1016/S0969-8051(02)00419-5
66. Andreopoulos D, Kasi LP, Asimacopoulos PJ, Jhingran SG, Cole W, Yang D, et al. Selective *in vitro* labeling of white blood cells using 99mTc-labeled liposomes. *Nucl Med Biol* 2002; **29**: 185–90. doi: 10.1016/S0969-8051(01)00299-2
67. Oyen WJ, Boerman OC, Storm G, van Bloois L, Koenders EB, Claessens RA, et al. Detecting infection and inflammation with technetium-99m-labeled Stealth liposomes. *J Nucl Med* 1996; **37**: 1392–7.
68. Elbayoumi TA, Torchilin VP. Enhanced accumulation of long-circulating liposomes modified with the nucleosome-specific monoclonal antibody 2C5 in various tumours in mice: gamma-imaging studies. *Eur J Nucl Med Mol Imaging* 2006; **33**: 1196–205. doi: 10.1007/s00259-006-0139-x
69. Schiffelers RM, Koning GA, ten Hagen TL, Fens MH, Schraa AJ, Janssen AP, et al. Anti-tumor efficacy of tumor vasculature-targeted liposomal doxorubicin. *J Control Release* 2003; **91**: 115–22. doi: 10.1016/S0168-3659(03)00240-2
70. Kovacs L, Tassano M, Cabrera M, Fernandez M, Porcal W, Anjos RM, et al. Labeling polyamidoamine (PAMAM) dendrimers with technetium-99m via hydrazinonicotinamide (HYNIC). *Curr Radiopharm* 2014; **7**: 115–22.
71. Khosroshahi AG, Amanlou M, Sabzevari O, Daha FJ, Aghasadeghi MR, Ghorbani M, et al. A comparative study of two novel nanosized radiolabeled analogues of methionine for SPECT tumour imaging. *Curr Med Chem* 2013; **20**: 123–33. doi: 10.2174/092986731130201012
72. Kobayashi H, Sato N, Saga T, Nakamoto Y, Ishimori T, Toyama S, et al. Monoclonal antibody-dendrimer conjugates enable radiolabeling of antibody with markedly high specific activity with minimal loss of immunoreactivity. *Eur J Nucl Med* 2000; **27**: 1334–9. doi: 10.1007/s002590000293
73. Kobayashi H, Wu C, Kim MK, Paik CH, Carrasquillo JA, Brechbiel MW. Evaluation of the *in vivo* biodistribution of indium-111 and yttrium-88 labeled dendrimer-1B4M-DTPA and its conjugation with anti-Tac monoclonal antibody. *Bioconjug Chem* 1999; **10**: 103–11. doi: 10.1021/bc980091d
74. Amirkhanov NV, Zhang K, Aruva MR, Thakur ML, Wickstrom E. Imaging human pancreatic cancer xenografts by targeting mutant KRAS2 mRNA with [(111)In]DOTA(n)-poly(diamidopropanoyl)(m)-KRAS2 PNA-D(Cys-Ser-Lys-Cys) nanoparticles. *Bioconjug Chem* 2010; **21**: 731–40. doi: 10.1021/bc900523c
75. Das M, Datir SR, Singh RP, Jain S. Augmented anticancer activity of a targeted, intracellularly activatable, theranostic nanomedicine based on fluorescent and radiolabeled, methotrexate-folic Acid-multiwalled carbon nanotube conjugate. *Mol Pharm* 2013; **10**: 2543–57. doi: 10.1021/mp300701e
76. Jimenez-Mancilla N, Ferro-Flores G, Santos-Cuevas C, Ocampo-Garcia B, Luna-Gutierrez M, Azorin-Vega E, et al. Multifunctional targeted therapy system based on (99m) Tc/(177) Lu-labeled gold nanoparticles-Tat(49-57)-Lys(3) -bombesin internalized in nuclei of prostate cancer cells. *J Labelled Comp Radiopharm* 2013; **56**: 663–71.
77. Morales-Avila E, Ferro-Flores G, Ocampo-Garcia BE, De Leon-Rodriguez LM, Santos-Cuevas CL, Garcia-Becerra R, et al. Multimeric system of 99mTc-labeled gold nanoparticles conjugated to c[RGDfK(C)] for molecular imaging of tumor alpha(v) beta(3) expression. *Bioconjug Chem* 2011; **22**: 913–22. doi: 10.1021/bc100551s
78. Zhang G, Yang Z, Lu W, Zhang R, Huang Q, Tian M, et al. Influence of anchoring ligands and particle size on the colloidal stability and *in vivo* biodistribution of polyethylene glycol-coated gold nanoparticles in tumor-xenografted mice. *Biomaterials* 2009; **30**: 1928–36. doi: 10.1016/j.biomaterials.2008.12.038
79. Bogdanov AA Jr, Gupta S, Koshkina N, Corr SJ, Zhang S, Curley SA, et al. Gold nanoparticles stabilized with MPEG-grafted poly(l-lysine): *in vitro* and *in vivo* evaluation of a potential theranostic agent. *Bioconjug Chem* 2015; **26**: 39–50. doi: 10.1021/bc5005087
80. Oberdorster G, Oberdorster E, Oberdorster J. Nanotoxicology: an emerging discipline evolving from studies of ultrafine particles. *Environ Health Perspect* 2005; **113**: 823–39.
81. Zhang X. Gold nanoparticles: recent advances in the biomedical applications. *Cell Biochem Biophys* 2015; **72**: 771–5. doi: 10.1007/s12013-015-0529-4
82. Mariani G, Moresco L, Viale G, Villa G, Bagnasco M, Canavese G, et al. Radioguided sentinel lymph node biopsy in breast cancer surgery. *J Nucl Med* 2001; **42**: 1198–215.
83. Seo Y, Aparici CM, Chen CP, Hsu C, Kased N, Schreck C, et al. Mapping of lymphatic drainage from the prostate using filtered 99mTc-sulfur nanocolloid and SPECT/CT. *J Nucl Med* 2011; **52**: 1068–72. doi: 10.2967/jnumed.110.085944
84. Ganswindt U, Schilling D, Muller AC, Bares R, Bartenstein P, Belka C. Distribution of prostate sentinel nodes: a SPECT-derived anatomic atlas. *Int J Radiat Oncol Biol Phys* 2011; **79**: 1364–72. doi: 10.1016/j.ijrobp.2010.01.012
85. Alazraki NP, Eshima D, Eshima LA, Herda SC, Murray DR, Vansant JP, et al. Lymphoscintigraphy, the sentinel node concept, and the intraoperative gamma probe in melanoma, breast cancer, and other potential cancers. *Semin Nucl Med* 1997; **27**: 55–67. doi: 10.1016/S0001-2998(97)80036-0
86. Khalifa A, Dodds D, Rampling R, Paterson J, Murray T. Liposomal distribution in malignant glioma: possibilities for therapy. *Nucl Med Commun* 1997; **18**: 17–23. doi: 10.1097/00006231-199701000-00005
87. Kubo A, Nakamura K, Sammiya T, Katayama M, Hashimoto T, Hashimoto S, et al. Indium-111-labelled liposomes: dosimetry and tumour detection in patients with cancer. *Eur J Nucl Med* 1993; **20**: 107–13. doi: 10.1007/BF00168869
88. Presant CA, Proffitt RT, Turner AF, Williams LE, Winsor D, Werner JL, et al. Successful imaging of human cancer with indium-111-labeled phospholipid vesicles. *Cancer* 1988; **62**: 905–11. doi: 10.1002/1097-0142(19880901)62:5<905::AID-CNCR2820620509>3.0.CO;2-3
89. Presant CA, Turner AF, Proffitt RT. Potential for improvement in clinical decision-making: tumor imaging with in-111 labeled liposomes results of a phase ii-iii study. *J Liposome Res* 1994; **4**: 985–1008. doi: 10.3109/08982109409018615
90. Presant CA, Blayney D, Proffitt RT, Turner AF, Williams LE, Nadel HI, et al. Preliminary report: imaging of Kaposi sarcoma and lymphoma in AIDS with indium-111-labelled liposomes. *Lancet* 1990; **335**: 1307–9. doi: 10.1016/0140-6736(90)91188-G
91. Harrington KJ, Lewanski CR, Stewart JS. Liposomes as vehicles for targeted therapy

of cancer. Part 2: clinical development. *Clin Oncol (R Coll Radiol)* 2000; **12**: 16–24.
92. Vallabhajosula S. Molecular imaging: radiopharmaceuticals for PET and SPECT. 2009; **1**: 1–371.
93. Lubberink M, Schneider H, Bergstrom M, Lundqvist H. Quantitative imaging and correction for cascade gamma radiation of 76Br with 2D and 3D PET. *Phys Med Biol* 2002; **47**: 3519–34. doi: 10.1088/0031-9155/47/19/306
94. Lubberink M, Herzog H. Quantitative imaging of 124I and 86Y with PET. *Eur J Nucl Med Mol Imaging* 2011; **38**(Suppl. 1): S10–18. doi: 10.1007/s00259-011-1768-2
95. Verel I, Visser GW, Boellaard R, Boerman OC, van Eerd J, Snow GB, et al. Quantitative 89Zr immuno-PET for *in vivo* scouting of 90Y-labeled monoclonal antibodies in xenograft-bearing nude mice. *J Nucl Med* 2003; **44**: 1663–70.
96. Billinge S. Materials science: nanoparticle structures served up on a tray. *Nature* 2013; **495**: 453–4. doi: 10.1038/495453a
97. Stockhofe K, Postema JM, Schieferstein H, Ross TL. Radiolabeling of nanoparticles and polymers for PET Imaging. *Pharmaceuticals (Basel)* 2014; **7**: 392–418. doi: 10.3390/ph7040392
98. Marik J, Tartis MS, Zhang H, Fung JY, Kheirolomoom A, Sutcliffe JL, et al. Long-circulating liposomes radiolabeled with [18F]fluorodipalmitin ([18F]FDP). *Nucl Med Biol* 2007; **34**: 165–71. doi: 10.1016/j.nucmedbio.2006.12.004
99. Wangler B, Kostikov AP, Niedermoser S, Chin J, Orchowski K, Schirrmacher E, et al. Protein labeling with the labeling precursor [(18)F]SiFA-SH for positron emission tomography. *Nat Protoc* 2012; **7**: 1964–9.
100. Jauregui-Osoro M, Williamson PA, Glaria A, Sunassee K, Charoenphun P, Green MA, et al. Biocompatible inorganic nanoparticles for [18F]-fluoride binding with applications in PET imaging. *Dalton Trans* 2011; **40**: 6226–37. doi: 10.1039/c0dt01618g
101. McBride WJ, Sharkey RM, Goldenberg DM. Radiofluorination using aluminum-fluoride (Al18F). *EJNMMI Res* 2013; **3**: 36. doi: 10.1186/2191-219X-3-36
102. Wadas TJ, Wong EH, Weisman GR, Anderson CJ. Coordinating radiometals of copper, gallium, indium, yttrium, and zirconium for PET and SPECT imaging of disease. *Chem Rev* 2010; **110**: 2858–902. doi: 10.1021/cr900325h
103. Petersen AL, Binderup T, Jolck RI, Rasmussen P, Henriksen JR, Pfeifer AK, et al. Positron emission tomography evaluation of somatostatin receptor targeted 64Cu-TATE-liposomes in a human neuroendocrine carcinoma mouse model. *J Control Release* 2012; **160**: 254–63. doi: 10.1016/j.jconrel.2011.12.038
104. Mahakian LM, Farwell DG, Zhang H, Seo JW, Poirier B, Tinling SP, et al. Comparison of PET imaging with 64Cu-liposomes and 18F-FDG in the 7,12-dimethylbenz[a]anthracene (DMBA)-induced hamster buccal pouch model of oral dysplasia and squamous cell carcinoma. *Mol Imaging Biol* 2014; **16**: 284–92. doi: 10.1007/s11307-013-0676-1
105. Tian M, Lu W, Zhang R, Xiong C, Ensor J, Nazario J, et al. Tumor uptake of hollow gold nanospheres after intravenous and intra-arterial injection: PET/CT study in a rabbit VX2 liver cancer model. *Mol Imaging Biol* 2013; **15**: 614–24. doi: 10.1007/s11307-013-0635-x
106. Nahrendorf M, Keliher E, Marinelli B, Waterman P, Feruglio PF, Fexon L, et al. Hybrid PET-optical imaging using targeted probes. *Proc Natl Acad Sci U S A* 2010; **107**: 7910–15. doi: 10.1073/pnas.0915163107
107. Ait-Mohand S, Fournier P, Dumulon-Perreault V, Kiefer GE, Jurek P, Ferreira CL, et al. Evaluation of 64Cu-labeled bifunctional chelate-bombesin conjugates. *Bioconjug Chem* 2011; **22**: 1729–35. doi: 10.1021/bc2002665
108. Tu C, Ma X, House A, Kauzlarich SM, Louie AY. PET imaging and biodistribution of silicon quantum dots in mice. *ACS Med Chem Lett* 2011; **2**: 285–8. doi: 10.1021/ml1002844
109. Torres Martin de Rosales R, Tavare R, Paul RL, Jauregui-Osoro M, Protti A, Glaria A, et al. Synthesis of 64Cu(II)-bis(dithiocarbamatebisphosphonate) and its conjugation with superparamagnetic iron oxide nanoparticles: *in vivo* evaluation as dual-modality PET-MRI agent. *Angew Chem Int Ed Engl* 2011; **50**: 5509–13. doi: 10.1002/anie.201007894
110. Deri MA, Zeglis BM, Francesconi LC, Lewis JS. PET imaging with $^{89}$Zr: from radiochemistry to the clinic. *Nucl Med Biol* 2013; **40**: 3–14. doi: 10.1016/j.nucmedbio.2012.08.004
111. Guerard F, Lee YS, Tripier R, Szajek LP, Deschamps JR, Brechbiel MW. Investigation of Zr(IV) and 89Zr(IV) complexation with hydroxamates: progress towards designing a better chelator than desferrioxamine B for immuno-PET imaging. *Chem Commun (Camb)* 2013; **49**: 1002–4.
112. Shaffer TM, Wall MA, Harmsen S, Longo VA, Drain CM, Kircher MF, et al. Silica nanoparticles as substrates for chelator-free labeling of oxophilic radioisotopes. *Nano Lett* 2015; **15**: 864–8. doi: 10.1021/nl503522y
113. Boros E, Bowen AM, Josephson L, Vasdev N, Holland JP. Chelate-free metal ion binding and heat-induced radiolabeling of iron oxide nanoparticles. *Chem Sci* 2015; **6**: 225–36. doi: 10.1039/C4SC02778G
114. Pérez-Campaña C, Gómez-Vallejo V, Puigivila M, Martin A, Calvo-Fernández T, Moya SE, et al. Biodistribution of different sized nanoparticles assessed by positron emission tomography: a general strategy for direct activation of metal oxide particles. *ACS Nano* 2013; **7**: 3498–505. doi: 10.1021/nn400450p
115. Oku N, Tokudome Y, Tsukada H, Kosugi T, Namba Y, Okada S. *In vivo* trafficking of long-circulating liposomes in tumour-bearing mice determined by positron emission tomography. *Biopharm Drug Dispos* 1996; **17**: 435–41. doi: 10.1002/(SICI)1099-081X(199607)17:5<435::AID-BDD435>3.0.CO;2-K
116. Benezra M, Hambardzumyan D, Penate-Medina O, Veach DR, Pillarsetty N, Smith-Jones P, et al. Fluorine-labeled dasatinib nanoformulations as targeted molecular imaging probes in a PDGFB-driven murine glioblastoma model. *Neoplasia* 2012; **14**: 1132–43. doi: 10.1593/neo.121750
117. Urakami T, Akai S, Katayama Y, Harada N, Tsukada H, Oku N. Novel amphiphilic probes for [18F]-radiolabeling preformed liposomes and determination of liposomal trafficking by positron emission tomography. *J Med Chem* 2007; **50**: 6454–7. doi: 10.1021/jm7010518
118. Zhu J, Chin J, Wangler C, Wangler B, Lennox RB, Schirrmacher R. Rapid (18)F-labeling and loading of PEGylated gold nanoparticles for *in vivo* applications. *Bioconjug Chem* 2014; **25**: 1143–50. doi: 10.1021/bc5001593
119. Zhou D, Kim SH, Carroll VM, Dence CS, Katzenellenbogen JA. Utilizing electrostatic interactions to facilitate F-18 radiolabeling of poly(amido)amine (PAMAM) dendrimers. *Org Biomol Chem* 2014; **12**: 8696–701. doi: 10.1039/c4ob01616e
120. Almutairi A, Rossin R, Shokeen M, Hagooly A, Ananth A, Capoccia B, et al. Biodegradable dendritic positron-emitting nanoprobes for the noninvasive imaging of angiogenesis. *Proc Natl Acad Sci U S A* 2009; **106**: 685–90. doi: 10.1073/pnas.0811757106
121. Benezra M, Penate-Medina O, Zanzonico PB, Schaer D, Ow H, Burns A, et al. Multimodal silica nanoparticles are effective cancer-targeted probes in a model of human melanoma. *J Clin Invest* 2011; **121**: 2768–80. doi: 10.1172/JCI45600
122. Frigell J, Garcia I, Gomez-Vallejo V, Llop J, Penades S. 68Ga-labeled gold

glyconanoparticles for exploring blood-brain barrier permeability: preparation, biodistribution studies, and improved brain uptake via neuropeptide conjugation. *J Am Chem Soc* 2014; **136**: 449–57. doi: 10.1021/ja411096m

123. Xie H, Wang ZJ, Bao A, Goins B, Phillips WT. *In vivo* PET imaging and biodistribution of radiolabeled gold nanoshells in rats with tumor xenografts. *Int J Pharm* 2010; **395**: 324–30. doi: 10.1016/j.ijpharm.2010.06.005
124. Hu H, Huang P, Weiss OJ, Yan X, Yue X, Zhang MG, et al. PET and NIR optical imaging using self-illuminating (64)Cu-doped chelator-free gold nanoclusters. *Biomaterials* 2014; **35**: 9868–76. doi: 10.1016/j.biomaterials.2014.08.038
125. Karmani L, Labar D, Valembois V, Bouchat V, Nagaswaran PG, Bol A, et al. Antibody-functionalized nanoparticles for imaging cancer: influence of conjugation to gold nanoparticles on the biodistribution of 89Zr-labeled cetuximab in mice. *Contrast Media Mol Imaging* 2013; **8**: 402–8. doi: 10.1002/cmmi.1539
126. Karmani L, Bouchat V, Bouzin C, Leveque P, Labar D, Bol A, et al. (89)Zr-labeled anti-endoglin antibody-targeted gold nanoparticles for imaging cancer: implications for future cancer therapy. *Nanomedicine (Lond)* 2014; **9**: 1923–37. doi: 10.2217/nnm.13.185
127. Papahadjopoulos D, Allen TM, Gabizon A, Mayhew E, Matthay K, Huang SK, et al. Sterically stabilized liposomes: improvements in pharmacokinetics and antitumor therapeutic efficacy. *Proc Natl Acad Sci U S A* 1991; **88**: 11460–4. doi: 10.1073/pnas.88.24.11460
128. Locke LW, Mayo MW, Yoo AD, Williams MB, Berr SS. PET imaging of tumor associated macrophages using mannose coated 64Cu liposomes. *Biomaterials* 2012; **33**: 7785–93. doi: 10.1016/j.biomaterials.2012.07.022
129. Petersen AL, Binderup T, Rasmussen P, Henriksen JR, Elema DR, Kjaer A, et al. 64Cu loaded liposomes as positron emission tomography imaging agents. *Biomaterials* 2011; **32**: 2334–41. doi: 10.1016/j.biomaterials.2010.11.059
130. Seo JW, Zhang H, Kukis DL, Meares CF, Ferrara KW. A novel method to label preformed liposomes with 64Cu for positron emission tomography (PET) imaging. *Bioconjug Chem* 2008; **19**: 2577–84. doi: 10.1021/bc8002937
131. Seo JW, Mahakian LM, Tam S, Qin S, Ingham ES, Meares CF, et al. The pharmacokinetics of Zr-89 labeled liposomes over extended periods in a murine tumor model. *Nucl Med Biol* 2015; **42**: 155–63. doi: 10.1016/j.nucmedbio.2014.09.001
132. Reubi JC, Schar JC, Waser B, Wenger S, Heppeler A, Schmitt JS, et al. Affinity profiles for human somatostatin receptor subtypes SST1-SST5 of somatostatin radiotracers selected for scintigraphic and radiotherapeutic use. *Eur J Nucl Med* 2000; **27**: 273–82. doi: 10.1007/s002590050034
133. Schipper ML, Iyer G, Koh AL, Cheng Z, Ebenstein Y, Aharoni A, et al. Particle size, surface coating, and PEGylation influence the biodistribution of quantum dots in living mice. *Small* 2009; **5**: 126–34. doi: 10.1002/smll.200800003
134. Keliher EJ, Yoo J, Nahrendorf M, Lewis JS, Marinelli B, Newton A, et al. 89Zr-labeled dextran nanoparticles allow *in vivo* macrophage imaging. *Bioconjug Chem* 2011; **22**: 2383–9. doi: 10.1021/bc200405d
135. Ruggiero A, Villa CH, Holland JP, Sprinkle SR, May C, Lewis JS, et al. Imaging and treating tumor vasculature with targeted radiolabeled carbon nanotubes. *Int J Nanomedicine* 2010; **5**: 783–802. doi: 10.2147/IJN.S13300
136. Nguyen QT, Tsien RY. Fluorescence-guided surgery with live molecular navigation—a new cutting edge. *Nat Rev Cancer* 2013; **13**: 653–62. doi: 10.1038/nrc3566
137. Fortuin AS, Barentsz JO. Comments on Ultrasmall superparamagnetic particles of iron oxide allow for the detection of metastases in normal sized pelvic lymph nodes of patients with bladder and/or prostate cancer, Triantafyllou et al., European Journal of Cancer, published online 22 October 2012. *Eur J Cancer* 2013; **49**: 1789–90. doi: 10.1016/j.ejca.2013.01.023
138. de Vries A, Kok MB, Sanders HM, Nicolay K, Strijkers GJ, Grull H. Multimodal liposomes for SPECT/MR imaging as a tool for in situ relaxivity measurements. *Contrast Media Mol Imaging* 2012; **7**: 68–75. doi: 10.1002/cmmi.468
139. Thorek DL, Chen AK, Czupryna J, Tsourkas A. Superparamagnetic iron oxide nanoparticle probes for molecular imaging. *Ann Biomed Eng* 2006; **34**: 23–38. doi: 10.1007/s10439-005-9002-7
140. Thorek DL, Ulmert D, Diop NF, Lupu ME, Doran MG, Huang R, et al. Non-invasive mapping of deep-tissue lymph nodes in live animals using a multimodal PET/MRI nanoparticle. *Nat Commun* 2014; **5**: 3097. doi: 10.1038/ncomms4097
141. Torres Martin de Rosales R, Tavare R, Glaria A, Varma G, Protti A, Blower PJ. ($^{99}$m)Tc-bisphosphonate-iron oxide nanoparticle conjugates for dual-modality biomedical imaging. *Bioconjug Chem* 2011; **22**: 455–65. doi: 10.1021/bc100483k
142. Devaraj NK, Keliher EJ, Thurber GM, Nahrendorf M, Weissleder R. 18F labeled nanoparticles for *in vivo* PET-CT imaging. *Bioconjug Chem* 2009; **20**: 397–401. doi: 10.1021/bc8004649
143. Nahrendorf M, Keliher E, Marinelli B, Leuschner F, Robbins CS, Gerszten RE, et al. Detection of macrophages in aortic aneurysms by nanoparticle positron emission tomography-computed tomography. *Arterioscler Thromb Vasc Biol* 2011; **31**: 750–7. doi: 10.1161/ATVBAHA.110.221499
144. Madru R, Tran TA, Axelsson J, Ingvar C, Bibic A, Stahlberg F, et al. (68)Ga-labeled superparamagnetic iron oxide nanoparticles (SPIONs) for multi-modality PET/MR/Cherenkov luminescence imaging of sentinel lymph nodes. *Am J Nucl Med Mol Imaging* 2013; **4**: 60–9.
145. Wong RM, Gilbert DA, Liu K, Louie AY. Rapid size-controlled synthesis of dextran-coated, 64Cu-doped iron oxide nanoparticles. *ACS Nano* 2012; **6**: 3461–7. doi: 10.1021/nn300494k
146. Jarrett BR, Gustafsson B, Kukis DL, Louie AY. Synthesis of 64Cu-labeled magnetic nanoparticles for multimodal imaging. *Bioconjug Chem* 2008; **19**: 1496–504. doi: 10.1021/bc800108v
147. Zhao S, Wu J, Wang C, Liu H, Dong X, Shi C, et al. Intraoperative fluorescence-guided resection of high-grade malignant gliomas using 5-aminolevulinic acid-induced porphyrins: a systematic review and meta-analysis of prospective studies. *PLoS One* 2013; **8**: e63682. doi: 10.1371/journal.pone.0063682
148. Duconge F, Pons T, Pestourie C, Herin L, Theze B, Gombert K, et al. Fluorine-18-labeled phospholipid quantum dot micelles for *in vivo* multimodal imaging from whole body to cellular scales. *Bioconjug Chem* 2008; **19**: 1921–6. doi: 10.1021/bc800179j
149. Stelter L, Pinkernelle JG, Michel R, Schwartlander R, Raschzok N, Morgul MH, et al. Modification of aminosilanized superparamagnetic nanoparticles: feasibility of multimodal detection using 3T MRI, small animal PET, and fluorescence imaging. *Mol Imaging Biol* 2010; **12**: 25–34. doi: 10.1007/s11307-009-0237-9
150. Nahrendorf M, Zhang H, Hembrador S, Panizzi P, Sosnovik DE, Aikawa E, et al. Nanoparticle PET-CT imaging of macrophages in inflammatory atherosclerosis. *Circulation* 2008; **117**: 379–87. doi: 10.1161/CIRCULATIONAHA.107.741181
151. Cai W, Chen K, Li ZB, Gambhir SS, Chen X. Dual-function probe for PET and near-infrared

fluorescence imaging of tumour vasculature. *J Nucl Med* 2007; **48**: 1862–70. doi: 10.2967/jnumed.107.043216

152. Cherenkov PA. Visible emission of clean liquids by action of γ radiation. *Doklady Akademii Nauk SSSR* 1934; **2**: 451.
153. Boschi F, Spinelli AE. Quantum dots excitation using pure beta minus radioisotopes emitting Cerenkov radiation. *RSC Adv* 2012; **2**: 11049–52. doi: 10.1039/c2ra22101b
154. Beattie BJ, Thorek DL, Schmidtlein CR, Pentlow KS, Humm JL, Hielscher AH. Quantitative modeling of Cerenkov light production efficiency from medical radionuclides. *PLoS One* 2012; **7**: e31402. doi: 10.1371/journal.pone.0031402
155. Thorek DL, Abou DS, Beattie BJ, Bartlett RM, Huang R, Zanzonico PB, et al. Positron lymphography: multimodal, high-resolution, dynamic mapping and resection of lymph nodes after intradermal injection of 18F-FDG. *J Nucl Med* 2012; **53**: 1438–45. doi: 10.2967/jnumed.112.104349
156. Ruggiero A, Holland JP, Lewis JS, Grimm J. Cerenkov luminescence imaging of medical isotopes. *J Nucl Med* 2010; **51**: 1123–30. doi: 10.2967/jnumed.110.076521
157. Liu H, Carpenter CM, Jiang H, Pratx G, Sun C, Buchin MP, et al. Intraoperative imaging of tumours using Cerenkov luminescence endoscopy: a feasibility experimental study. *J Nucl Med* 2012; **53**: 1579–84. doi: 10.2967/jnumed.111.098541
158. Park JC, Yu MK, An GI, Park SI, Oh J, Kim HJ, et al. Facile preparation of a hybrid nanoprobe for triple-modality optical/PET/MR imaging. *Small* 2010; **6**: 2863–8. doi: 10.1002/smll.201001418
159. Kim J, Pandya DN, Lee W, Park JW, Kim YJ, Kwak W, et al. Vivid tumour imaging utilizing liposome-carried bimodal radiotracer. *ACS Med Chem Lett* 2014; **5**: 390–4. doi: 10.1021/ml400513g
160. Grahame R, Ramsey NW, Scott JT. Radioactive colloidal gold. In chronic knee effusions with Baker's cyst formation. *Ann Rheum Dis* 1970; **29**: 159–63. doi: 10.1136/ard.29.2.159
161. Metz O, Stoll W, Plenert W. Meningosis prophylaxis with intrathecal 198Au-colloid and methotrexate in childhood acute lymphocytic leukemia. *Cancer* 1982; **49**: 224–8. doi: 10.1002/1097-0142(19820115)49:2<224::AID-CNCR2820490205>3.0.CO;2-O
162. Black KC, Wang Y, Luehmann HP, Cai X, Xing W, Pang B, et al. Radioactive 198Au-doped nanostructures with different shapes for *in vivo* analyses of their biodistribution, tumor uptake, and intratumoral distribution. *ACS Nano* 2014; **8**: 4385–94. doi: 10.1021/nn406258m
163. Thorek DL, Ogirala A, Beattie BJ, Grimm J. Quantitative imaging of disease signatures through radioactive decay signal conversion. *Nat Med* 2013; **19**: 1345–50. doi: 10.1038/nm.3323
164. Kotagiri N, Niedzwiedzki DM, Ohara K, Achilefu S. Activatable probes based on distance-dependent luminescence associated with Cerenkov radiation. *Angew Chem Int Ed Engl* 2013; **52**: 7756–60. doi: 10.1002/anie.201302564
165. Thorek DL, Das S, Grimm J. Molecular imaging using nanoparticle quenchers of Cerenkov luminescence. *Small* 2014; **10**: 3729–34. doi: 10.1002/smll.201400733
166. Dothager RS, Goiffon RJ, Jackson E, Harpstrite S, Piwnica-Worms D. Cerenkov radiation energy transfer (CRET) imaging: a novel method for optical imaging of PET isotopes in biological systems. *PLoS One* 2010; **5**: e13300. doi: 10.1371/journal.pone.0013300
167. Liu H, Zhang X, Xing B, Han P, Gambhir SS, Cheng Z. Radiation-luminescence-excited quantum dots for *in vivo* multiplexed optical imaging. *Small* 2010; **6**: 1087–91. doi: 10.1002/smll.200902408